A&A 667, A158 (2022)
https://doi.org/10.1051/0004-6361/202244197

Astronomy & Astrophysics

Data on 824 fireballs observed by the digital cameras of the European Fireball Network in 2017–2018

II. Analysis of orbital and physical properties of centimeter-sized meteoroids*

J. Borovička, P. Spurný, and L. Shrbený

Astronomical Institute of the Czech Academy of Sciences, Fričova 298, 25165 Ondřejov, Czech Republic
e-mail: jiri.borovicka@asu.cas.cz

Received 6 June 2022 / Accepted 6 September 2022

ABSTRACT

Meteoroids impacting the Earth on a daily basis are fragments of asteroids and comets. By studying fireballs produced during their disintegration in the atmosphere, we can gain information about their source regions and the properties of their parent bodies. In this work, data on 824 fireballs presented in an accompanying paper and catalog are used. We propose a new empirical parameter for the classification of the physical properties of meteoroids, based on the maximum dynamic pressure suffered by the meteoroid in the atmosphere. We then compare the physical and orbital properties of meteoroids. We find that aphelion distance is a better indicator of asteroidal origin than the Tisserand parameter. Meteoroids with aphelia lower than 4.9 AU are mostly asteroidal, with the exception of the Taurids and α Capricornids associated with the comets 2P/Encke and 169P/NEAT, respectively. We found another population of strong meteoroids of probably asteroidal origin on orbits with either high eccentricities or high inclinations, and aphelia up to ≈ 7 AU. Among the meteoroid streams, the Geminids and η Virginids are the strongest, and Leonids and α Capricornids the weakest. We found fine orbital structures within the Geminid and Perseid streams. Four minor meteoroid streams from the working list of the International Astronomical Union were confirmed. No meteoroid with perihelion distance lower than 0.07 AU was detected. Spectra are available for some of the fireballs, and they enabled us to identify several iron meteoroids and meteoroids deficient in sodium. Recognition and frequency of fireballs leading to meteorite falls is also discussed.

Key words. meteorites, meteors, meteoroids – catalogs

1. Introduction

This paper is the second of two papers devoted to the fireballs observed by the European Fireball Network in 2017–2018. The first paper (Borovička et al. 2022, hereafter Paper I) presented the motivation for the work, a brief history and the current status of the European Fireball Network, a description of the main instrument of the network, the Digital Autonomous Fireball Observatory (DAFO), the methods of data analysis, an explanation of all catalog entries, and a statistical evaluation of the whole sample of 824 fireballs. The catalog itself is available at the Centre de Données astronomiques de Strasbourg (CDS; see Paper I).

As shown in Paper I, the network is capable of detecting meteors brighter than absolute magnitude of about −2. Consequently, meteoroids of masses from about 5 g are detected for all entry velocities. In cases of high entry velocity ($\sim 70\,\mathrm{km\,s^{-1}}$), meteoroids with masses as low as 0.05 g can be detected. On the other end of the mass range, the brightest observed fireball in the 2-yr period reached a magnitude of −14 and the largest meteoroid had a mass of slightly more than 100 kg. From the total sample of 824 fireballs, 222 belonged to one of 16 major meteor showers. Most represented were the Taurids, Perseids, and Geminids, which together accounted for 164 fireballs.

The cataloged data for each fireball include date and time, atmospheric trajectory, initial and terminal velocity, radiant, heliocentric orbit, suggested shower membership, possible related body (asteroid or comet), maximum dynamic pressure along the trajectory, and terminal dynamic mass. Photometric data are given for all fireballs except for two that were observed during twilight. They include maximum brightness, total radiated energy, and derived quantities such as initial photometric mass and physical classification (see below). Information on the availability of spectral data is also provided and unusual spectra (irons, and sodium-deficient and sodium-rich spectra) are marked.

The purpose of this paper is to analyze the obtained fireball data. The main goal is to compare the orbital and physical properties of meteoroids. First, we derive a new measure of meteoroid physical properties based on the maximum dynamic pressure, which we compare with the classical P_E criterion of Ceplecha & McCrosky (1976) based on fireball end height. We evaluate orbits according to the Tisserand parameter and aphelion distance, but considering also other orbital elements. We search the orbits occupied mostly by structurally strong (asteroidal) and structurally weak (cometary) meteoroids. We compare the physical properties of meteoroids from different showers, and we discuss the extreme orbits with low perihelion distances or eccentricities above unity.

To further exploit the data, we study the radiants and orbits of meteor showers. Previous work on the Taurids (Spurný et al. 2017) have shown that the precision of data from DAFO is higher than that of other systems, and new structures within meteoroid streams can be revealed. We also examine if some not yet established meteor showers can be confirmed. The last two

* The catalog is available at the CDS via anonymous ftp to cdsarc.cds.unistra.fr (130.79.128.5) or via https://cdsarc.cds.unistra.fr/viz-bin/cat/J/A+A/667/A157

discussed topics are the identification of probable meteorite falls and relation of some meteoroids to specific asteroids.

2. Alternative physical classification of fireballs

The P_E criterion of Ceplecha & McCrosky (1976) has traditionally been used for fireball classification, that is for the evaluation of the physical properties of meteoroids. As explained in Paper I, it is computed as

$$P_E = \log \rho_e - 0.42 \log m_{phot76} + 1.49 \log v_\infty - 1.29 \log \cos z_R, \quad (1)$$

where ρ_e is the atmospheric density at the fireball end height in g cm^{-3}, m_{phot76} is the photometric mass in grams computed using the original luminous efficiency, τ_{76} (see Paper I for details), v_∞ is the entry velocity in km s^{-1}, and z_R is the zenith distance of the apparent radiant. Four fireball types, I, II, IIIA, and IIIB (from the strongest to the weakest), were defined, the boundary P_E values being −4.60, −5.25, and −5.70.

Other criteria were also proposed. Ceplecha (1988) mentioned the A_L criterion, which is equivalent to P_E, but used the total radiated light instead of the photometric mass. He also listed the ablation coefficient as a possible classification criterion, since the ablation coefficient is smallest for type I fireballs and largest for type IIIB fireballs. Ceplecha et al. (1993) proposed a two-dimensional classification with dynamic pressure at the fragmentation point forming the second dimension. The fragmentation point was found from a careful analysis of deceleration, requiring precise dynamic data. Trigo-Rodríguez & Llorca (2006), on the other hand, used the dynamic pressure at the point of maximum brightness to estimate the strength of cometary meteoroids. Borovička & Spurný (2020) and Borovička et al. (2020) used deceleration and detailed radiometric light curves to reveal multiple fragmentation points along fireball trajectories, and to study strength distribution inside meteoroids.

Fragmentation analysis is a time-consuming process and requires detailed data. The ablation coefficient was computed for many fireballs during the physical fit of velocity but it often has large uncertainty and for short fireballs it could not be computed at all. The maximum dynamic pressure, on the other hand, was computed for all fireballs. We were therefore interested to know if a simple fireball classification can be build on the basis of maximum dynamic pressure, p_{max}, instead of end height. One reason is that p_{max} is a more robust quantity, with end height being more dependent on observing circumstances.

It can be expected that p_{max}, similarly to end height, will depend on the trajectory slope, since under otherwise equal conditions, meteoroids on steep trajectories will penetrate deeper than meteoroids on shallow trajectories. Therefore, $p_{max}/\cos z$, where z is the average zenith distance of the radiant, is plotted in Fig. 1 as a function of photometric mass. It can be seen that the maximum pressure reached, not surprisingly, increases with meteoroid mass, m. One can indeed expect that larger pieces of a given material will penetrate deeper. The trend of the data, including the upper and the lower envelopes (not considering a few outliers), follows a dependency $p_{max}/\cos z \sim m^{1/3}$. Figure 1 also shows data without the $\cos z$ factor. It can be seen that the inclusion of $\cos z$ makes the range of pressures narrower. The lowest observed maximal pressures obviously belong to fireballs on shallow trajectories.

To reveal material properties from dynamic pressure, meteoroid mass must, therefore, be taken into account. The combined quantity $p_{max}/(m^{1/3}\cos z)$ is plotted in Fig. 2 as a function of entry velocity, v. One might expect no dependence on velocity because velocity is already contained in the computation of dynamic pressure. The plot, nevertheless, shows a clear dependence on velocity, well approximated by $\sim v^{3/2}$. It is not the purpose of this paper to explain the physics behind the dependency.

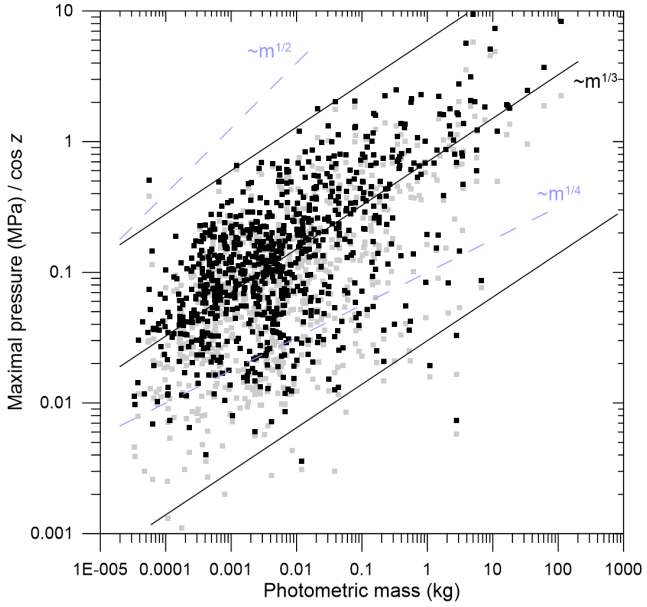

Fig. 1. Maximum dynamic pressure divided by the cosine of radiant zenith distance as a function of photometric mass for 822 fireballs. The light gray symbols represent the pressures without the $\cos z$ factor for the same fireballs. Solid lines represent the dependency on the cube root of mass ($m^{1/3}$) for the bulk of the data, the upper envelope (the strongest meteoroids), and the lower envelope (the weakest meteoroids). Dashed lines show dependencies on $m^{1/2}$ and $m^{1/4}$ for comparison. These dependencies do not correspond to the data.

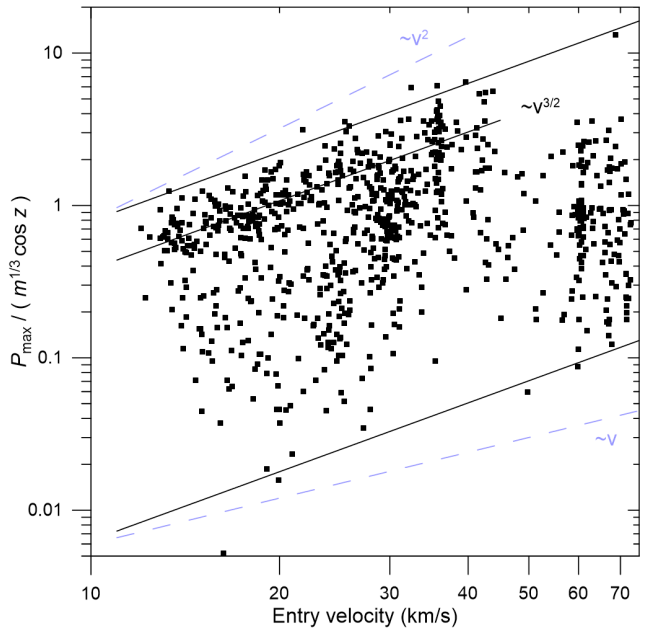

Fig. 2. Maximum dynamic pressure divided by the cosine of radiant zenith distance and cubic root of mass as a function of entry velocity for 822 fireballs. Solid lines represent the dependency on the 1.5th power of velocity ($v^{3/2}$) for the bulk of slow fireballs, the upper envelope (the strongest meteoroids), and the lower envelope (the weakest meteoroids). Dashed lines show dependencies on v^2 and v for comparison. These dependencies do not correspond to the data.

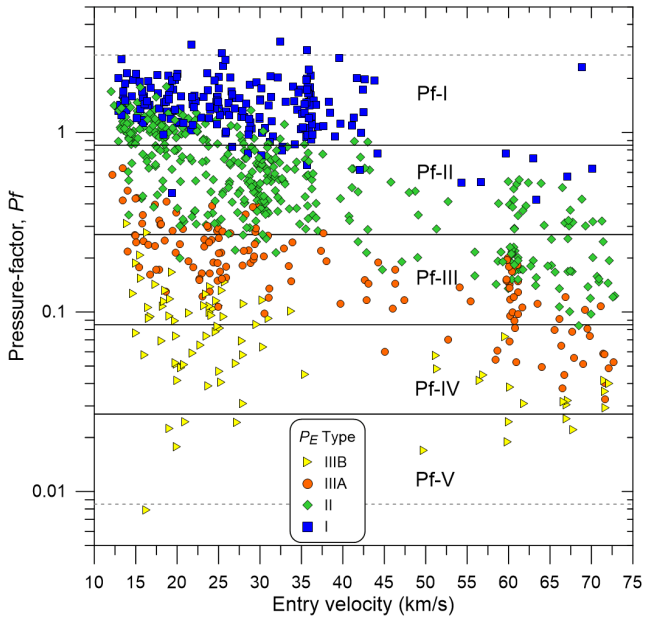

Fig. 3. Pressure factor defined by Eq. (2) as a function of entry velocity. The division of fireballs into five strength categories Pf-I to Pf-V is shown. The color symbols indicate the P_E type according to its definition.

It can be expected that the final fragmentation occurs when the dynamic pressure reaches the material strength. It is possible that fireballs with higher velocities have a higher chance of reaching an even higher dynamic pressure before the fragments are finally decelerated.

Nevertheless, by finding the dependence on mass and velocity, we can now define a new parameter for the evaluation of material strength based on the maximal dynamic pressure. We will call it the "pressure resistance factor" or simply the "pressure factor", abbreviated as Pf. It is defined as

$$Pf = 100\ p_{\max}\ \cos^{-1}z\ m_{\rm phot}^{-1/3}\ v_\infty^{-3/2}, \tag{2}$$

where $p_{\max}$ is the maximal dynamic pressure in MPa, z is the average zenith distance of the radiant (i.e., trajectory slope from the vertical), $m_{\rm phot}$ is the initial photometric mass in kg (see Paper I for the used luminous efficiency), and v_∞ is the entry velocity in km s^{-1}. As an example, Pf is equal to one for a meteoroid with an initial mass of 1 kg, which entered the atmosphere on a vertical trajectory with a speed of 21.5 km s^{-1} and reached a maximal dynamic pressure of 1 MPa.

Figure 3 shows the distribution of Pf values as a function of velocity. The Pf values are in the range from about 0.008 to three. There is no obvious grouping of Pf values. Nevertheless, for easier referencing, we defined five strength categories, designated Pf-I to Pf-V. The boundaries are marked in Fig. 3 and their numerical values are as follows:

$$\begin{aligned}
\text{Pf-I} &: 0.85 < Pf, \\
\text{Pf-II} &: 0.27 < Pf \le 0.85, \\
\text{Pf-III} &: 0.085 < Pf \le 0.27, \\
\text{Pf-IV} &: 0.027 < Pf \le 0.085, \\
\text{Pf-V} &: \quad Pf \le 0.027.
\end{aligned} \tag{3}$$

The sizes of categories Pf-II, Pf-III, and Pf-IV are equal in the logarithmic graph, and correspond to half of an order of magnitude. Most fireballs in categories Pf-I and Pf-V also fall in the interval of the same size (marked by dashed lines in Fig. 3). There are only a few exceptions that lie outside. No special categories were defined for them. In fact, there are only a few fireballs in the weakest category, Pf-V. Interestingly, there is a distinct upper limit of strength of fast fireballs (>45 km s^{-1}), which is exceeded in only one case. The boundaries of categories were chosen so that this limit forms the upper boundary of category Pf-II. The width of the categories was set so that the lower boundary of Pf-III corresponds to a Pf 10× lower than the upper boundary of Pf-II. This way, almost the whole group of fireballs with velocities about 60 km s^{-1} (mostly Perseids) falls into Pf-III. By necessity, however, there are many fireballs near the boundaries. The P_E classification has the same problem.

Figure 3 can also be used to compare the Pf and P_E classifications. Obviously, there is a different correction for velocity. While there are eight fireballs with velocities above 50 km s^{-1} classified as type I, there is only one Pf-I. Similarly, many high-velocity fireballs classified as type II fall into Pf-III. On the contrary, there are a number of slow type II fireballs that fall into Pf-I. We further investigate these differences in the next section, where physical and orbital classifications are compared.

3. Relation between orbital and physical properties

3.1. P_E and Pf parameters as a function of the Tisserand parameter

One of the most widespread methods for classifying orbits of Solar System bodies is that based on the Tisserand parameter (Tancredi 2014). Figure 4 shows both the P_E parameter and Pf in relation to the Tisserand parameter, T_J. Both plots look similar but there are notable differences. Using P_E, we would conclude the strongest observed body was a small meteoroid on a Halley-type orbit ($T_J < 2$). A number of Halley-type bodies have comparable P_E with meteoroids on evolved orbits with $T_J > 5$, which often fall into type II. Most of the weakest bodies with $P_E < -6$ are on Jupiter-family orbits ($2 < T_J < 3$). Although we do not know a priori the properties of meteoroids on different orbits, the plot of Pf with T_J better satisfies the expectation that bodies on cometary Halley-type orbits are generally weaker than bodies on asteroidal obits with high T_J. The number of extremely weak Jupiter-family meteoroids is also lower in this plot. We therefore consider Pf to be a better proxy of meteoroid physical properties (more specifically, resistance to ablation and fragmentation, which is probably connected to density, porosity, mechanical strength, or melting temperature), and Pf will therefore be used from this point on, rather than P_E.

3.2. Pf and spectra

Figure 5 shows the same plot as in Fig. 4b, but only for fireballs with good spectra. A remarkable group is five fireballs with iron spectra. All of them are on asteroidal orbits and have a significantly lower Pf than fireballs with normal (chondritic) spectra (and the same T_J). This fact was already stressed and explained by Vojáček et al. (2020). Metallic meteoroids with an iron–nickel composition melt easily and efficiently lose mass in the form of liquid droplets. It is therefore somewhat inappropriate to call meteoroids with a high Pf "strong" and those with a low Pf "weak", since irons are not weak. Better descriptions could perhaps be "resistant" and "susceptible" (to ablation).

In contrast to irons, there are three meteoroids deficient in sodium (but containing magnesium, in contrast to irons) on cometary orbits, which have quite a high Pf. Their nature is

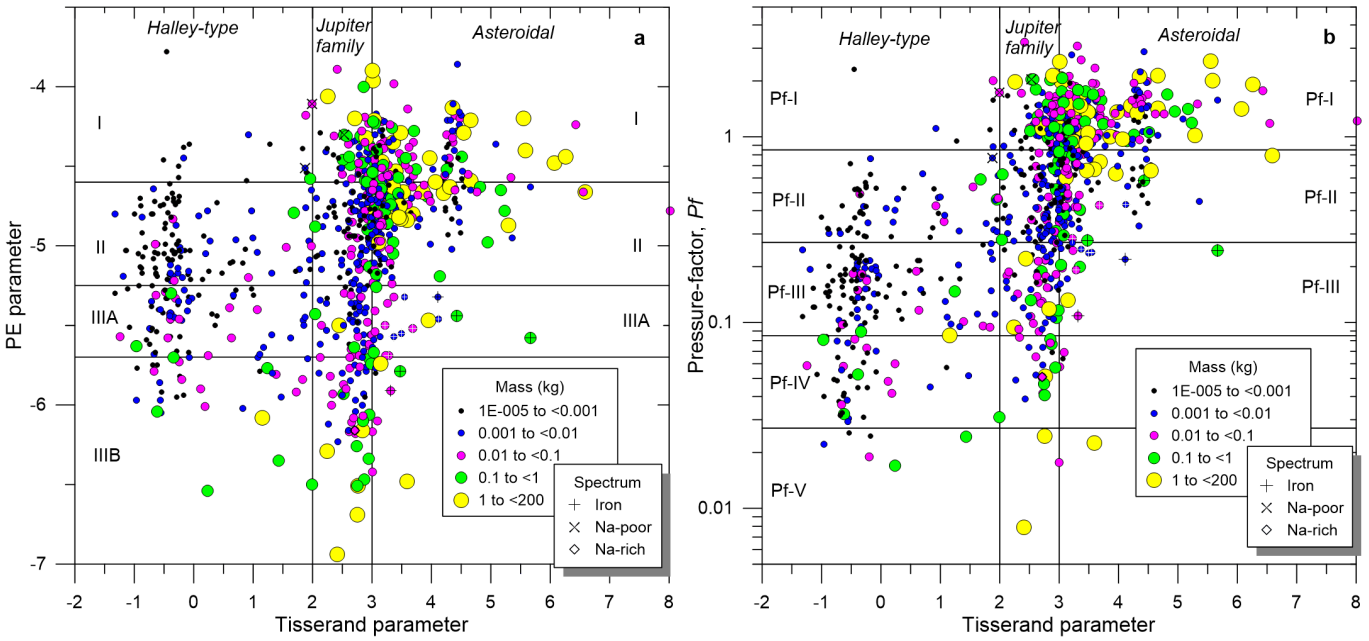

Fig. 4. Comparison of orbital and physical classification of fireballs using two physical classification schemes. The Tisserand parameter with respect to Jupiter is compared with the P_E parameter in *panel a* and with *Pf* in *panel b*. Symbol sizes and colors distinguish five intervals of meteoroid masses. Fireballs with unusual spectra are also marked. For most fireballs, however, spectra are not available. Fireballs supposed to be irons on the basis of other criteria (see Sect. 3.4) are marked by white crosses.

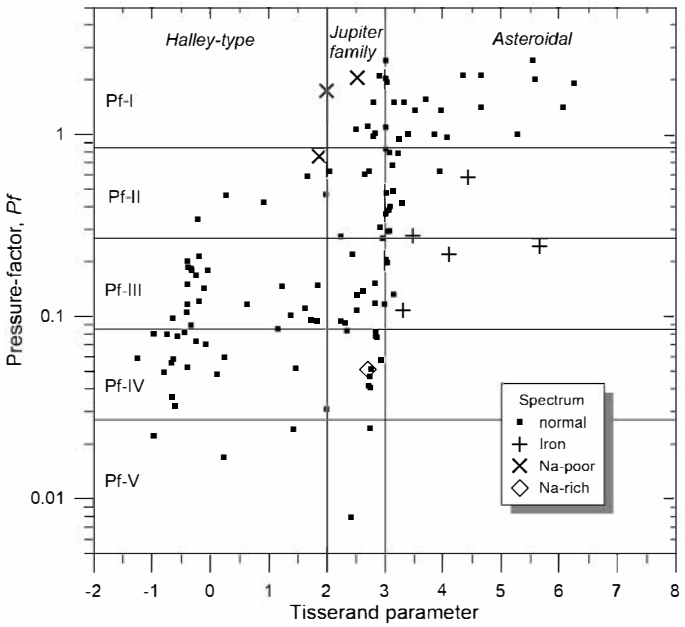

Fig. 5. Pressure factor as a function of the Tisserand parameter for fireballs with good spectra. Unusual spectra are shown with different symbols.

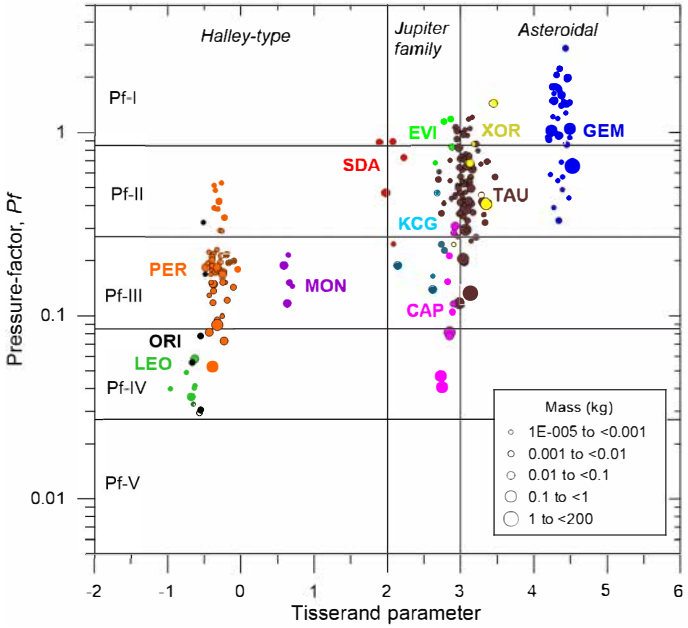

Fig. 6. Pressure factor as a function of the Tisserand parameter for fireballs belonging to major meteor showers. Only showers with at least four fireballs are shown. Colors are used to discriminate between different showers. Symbol sizes mark five intervals of meteoroid masses.

currently unclear. Finally, there is one fireball with an unusually bright sodium line on a Jupiter-family orbit. Its *Pf* is rather low but not unusual for that type of orbit. A more detailed analysis of fireball spectra will be the subject of a future work.

3.3. Pf and showers

Figure 6 shows the same plot as in Fig. 4b, but for fireballs of major meteor showers. An obvious fact is that all showers with a sufficient number of fireballs (Geminids, Taurids, α Capricornids, Perseids) are inhomogeneous. The *Pf* values within a shower cover about an order of magnitude. In Taurids, there is a mass-sorting effect, which was already noted by Spurný et al. (2017) and studied in detail by Borovička & Spurný (2020). Small meteoroids are more resistant than large ones. It was found that most of the Taurid material is porous and fragile but it contains stronger inclusions, which can also

exist separately as small meteoroids (while the porous material cannot). It seems that the same effect is present in α Capricornids and possibly also in Perseids. But both α Capricornids and Perseids are more susceptible to ablation than Taurids, and their *Pf* is shifted to lower values. Geminids are the most resistant among shower meteoroids, a fact already known (e.g., Babadzhanov 2002). Their *Pf* reaches roughly three in some cases, which is comparable to the highest values in our sample. The mass sorting is not present, or is even opposite. As it can be seen in Fig. 6, the weakest Geminids are the small ones. Detailed fragmentation modeling is need to investigate Geminid structure.

Other showers are represented by only a few fireballs in our sample. It is worth mentioning that the η Virginids are quite resistant, despite their cometary orbit. Using data from additional years, Brček et al. (2021) have confirmed that this is also the case for large meteoroids. The physical properties of η Virginids are, therefore, more similar to Geminids than Taurids. Southern δ Aquariids are also relatively resistant, which may be connected with their low perihelion distance. While χ Orionids may be similar to Taurids, κ Cygnids seem to be less resistant (but more than α Capricornids). December Monocerotids are similar to Perseids. Leonids are more susceptible than Perseids on average (but resistant Leonids also exist, see Kokhirova & Borovička 2011).

Although it is simplified and preliminary, average shower meteoroids can be assigned to the following Pf categories:

Pf-I : GEM, EVI
Pf-II : TAU (except the large ones), XOR, SDA
Pf-III : PER, MON, KCG, TAU (large)
Pf-IV : ORI, LEO, CAP

3.4. Orbital domains of asteroidal and cometary meteoroids

Looking back at Fig. 4b, we see that there are many fireballs concentrated along the $T_J = 3$ line, which is considered a boundary between asteroidal and cometary orbits. Fireballs with a low *Pf* lie mostly on the cometary side of the boundary. Fireballs with a high *Pf* are found on both sides of the boundary. It therefore seems that there are many resistant meteoroids with orbits of Jupiter-family comet type. There are, however, other criteria for distinguishing cometary and asteroidal orbits. One of the simplest was proposed by Kresák (1969a), which is based on the aphelion distance Q and defines asteroidal orbits as those with $Q < 4.6$ AU. Figure 7 shows *Pf* as a function of Q. We can see here that the aphelion distance of the vast majority of resistant meteoroids is lower than the semimajor axis of Jupiter (5.2 AU). The most resistant ones indeed lie within 4.6 AU.

Figures 8 and 9 further explore the orbital domains of resistant and susceptible meteoroids. Figure 8 shows the eccentricities, e, and semimajor axes, a, around the boundary between asteroidal and Jupiter-family cometary orbits for meteoroids larger than 5 g. Near-Earth asteroids and comets taken from the Jet Propulsion Laboratory database[1] are shown for comparison. Only objects with a data-arc span larger than 90 days have been included.

We can see that meteoroids of various Pf classes are mixed, as there are asteroids and comets. In the whole sample, meteoroids of class Pf-I prevail (54%). Meteoroids of susceptible classes Pf-III to Pf-V form only 21% of all meteoroids (the rest is the intermediate type Pf-II). There is, however, an orbital

[1] https://ssd.jpl.nasa.gov/tools/sbdb_query.html, accessed October 26, 2021.

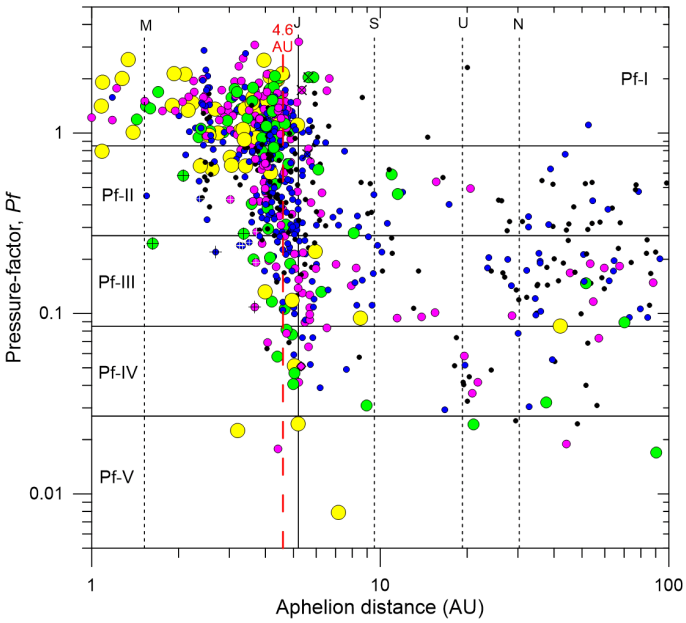

Fig. 7. Pressure factor as a function of aphelion distance. Fireballs with an aphelion distance larger than 100 AU are not shown. Meteoroid masses and spectra are marked as in Fig. 4. Vertical black lines indicate the semimajor axes of planets from Mars to Neptune. The dashed red line is drawn at 4.6 AU.

region, highlighted in yellow, where susceptible meteoroids form a majority (56%) and the Pf-I class is represented by only 16% of meteoroids. Comets are also more numerous than asteroids in this region. We therefore call it the comet domain.

The comet domain is defined by $Q > 4.9$ AU and $e < 0.9$ (for $a < 5$ AU). The other boundary for meteoroids, $q < 1$ AU, is due to the necessity of crossing the Earth's orbit to be observable. The boundaries are only approximate. In particular, the e-limit is poorly defined because there is little data near the boundary. In any case, high-eccentricity meteoroids with semimajor axes up to 3.5 AU are resistant, despite the fact that comets prevail over asteroids in this region. Comet 96/P Machholz 1 and several SOHO comets are here. The meteoroid resistance may be connected with their low perihelion distances of $q < 0.25$ AU. Some of these near-Sun meteoroids belong to the Southern and Northern δ Aquariid meteor showers.

The Q-limit nearly corresponds to the perihelion distance of Jupiter (4.95 AU). We note that there are susceptible cometary meteoroids below this limit also. The α Capricornids lie on both sides of the boundary but the majority are on the asteroidal side, similar to the comets 169P/NEAT and P/2003 T12 (SOHO). Taurids have even lower aphelia and also contain susceptible meteoroids, especially the large ones. They are related to comet 2P/Encke but occupy a large orbital space. The resonant branch contains a wide range of eccentricities at $a \sim 2.25$ AU while other Taurids have a variety of semimajor axes (Spurný et al. 2017).

Some of the susceptible sporadic meteoroids in the asteroidal orbital region are irons, but there are also truly weak, low-density meteoroids in asteroidal orbits. On the other hand, there seem also to be quite resistant meteoroids in the comet domain. Nevertheless, we also have to look at the orbital inclination, i, in Fig. 9. There are several resistant meteoroids (Pf-I) with semimajor axes 2.5–3.5 AU and large inclinations 40°–75°. Susceptible cometary meteoroids are rare in this region (only one with mass >5 g, two in the total sample). We therefore consider the comet domain to

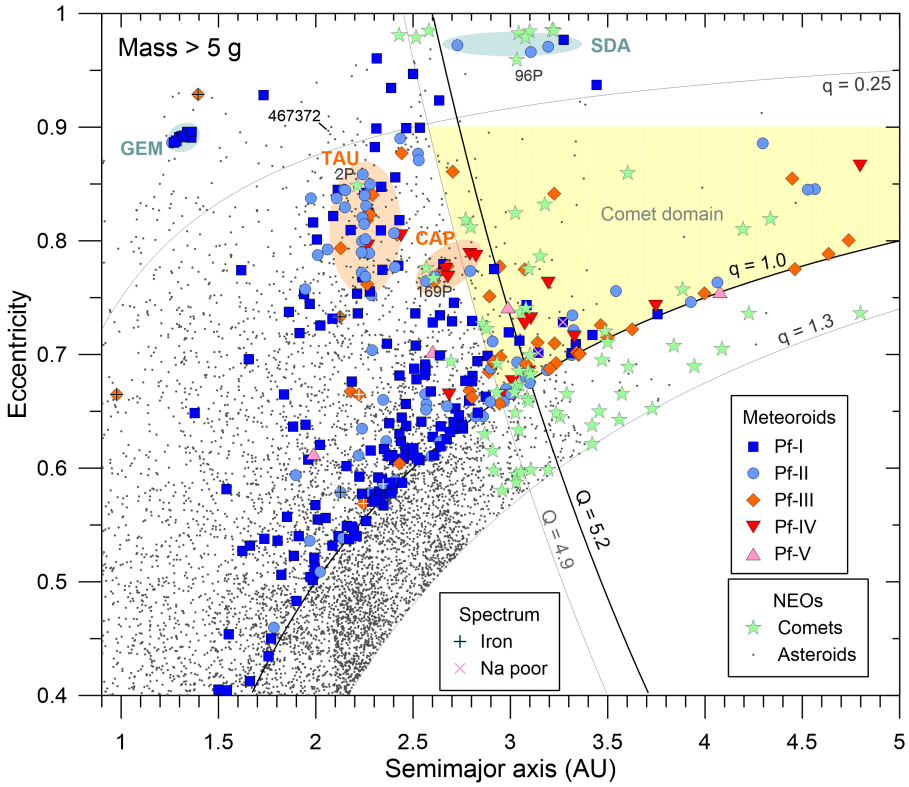

Fig. 8. Eccentricities and semimajor axes of meteoroids of various Pf classes and near-Earth objects (asteroids and comets with perihelion distance $q < 1.3$ AU). Semimajor axes (a) are restricted to 0.9–5 AU and eccentricities (e) to 0.4–1. All meteoroids with lower a or e are of class Pf-I, except two, which are Pf-II. Curves of constant perihelion (q) or aphelion (Q) distance are shown for selected values. Only meteoroids with masses larger than 5 g are shown. Regions where members of meteor showers Taurids (TAU), α Capricornids (CAP), Geminids (GEM), and Southern δ Aquariids (SDA) are found are highlighted (but not all meteoroids in that regions belong to the showers, and some shower members can be found also outside the regions). Meteoroids with iron or Na-poor spectra are marked. The region occupied primarily by comets and cometary meteoroids is highlighted in yellow.

be restricted to $i < 40°$ at semimajor axes around 3.5 AU. Then, only a few Pf-I meteoroids remain in the comet domain. Remarkably, most of them still have relatively high inclinations $\geq 20°$. Moreover, if spectra are known, they are deficient in sodium in these cases. Figure 9 shows only sporadic meteoroids.

Figure 10 extends Fig. 9 up to 600 AU in a and 180° in i. All observed meteoroids are shown. It is important to note that large semimajor axes have high uncertainties. Most meteoroids with $i \sim 113°$ are Perseids. The comet domain extends to all inclinations for $a \geq 5$ AU. There are only a few meteoroids classified as Pf-I with large semimajor axes ($a > 4$ AU).

We can conclude that asteroidal and cometary meteoroids are partly mixed in orbital space, as are asteroids and comets. Nevertheless, there are regions in the orbital space where mostly meteoroids susceptible to ablation and fragmentation are encountered. Since these regions overlap with those occupied primarily by comets, we can be confident that these meteoroids originate from comets. The domain of cometary meteoroids can be divided into a short-period one with:

$Q > 4.9$ AU,
$e < 0.9$ (or, possibly, $q > 0.25$ AU),
$i < 40°$,
$a < 5$ AU,

and a long-period one with:

$a > 5$ AU.

Asteroidal meteoroids are primarily encountered in orbits with lower aphelia ($Q < 4.9$ AU), or in orbits with somewhat larger aphelia (up to about 7 AU) but with either low perihelia ($q < 0.25$ AU) or high inclinations ($i > 40°$). A special sort of asteroidal meteoroids are irons, which are susceptible to ablation because they are readily melted.

Meteoroids considered as asteroidal are primarily those of class Pf-I with $Pf > 0.85$. Meteoroids of classes Pf-III to Pf-V with $Pf < 0.27$ are considered as cometary (except irons). Meteoroids of class Pf-II can be of both asteroidal and cometary origin. In comets, they are mostly, but not exclusively, encountered as small bodies with masses below 10 g. In fact, the distinction between cometary and asteroidal bodies according to Pf parameter is more evident for larger bodies. But regardless of mass, looking at Fig. 7, we can see that meteoroids with $Pf > 0.6$ are still mostly asteroidal. Nevertheless, as noted above, asteroidal meteoroids in cometary orbits and cometary meteoroids in asteroidal orbits can be encountered.

The five identified irons have a Pf in a relatively wide range, 0.1–0.6. Irons can be unambiguously distinguished according to their spectra. They are also characterized by smooth radiometric light curves with sudden ends (Vojáček et al. 2020). Because of their high meteoroid density, deceleration is low. Because of the lack of Na and Mg lines, fireballs appear rather bluish in color photographs. Based on these criteria, we identified seven fireballs with unavailable spectra that were likely caused by iron meteoroids. They are listed in Table 1 and marked by white

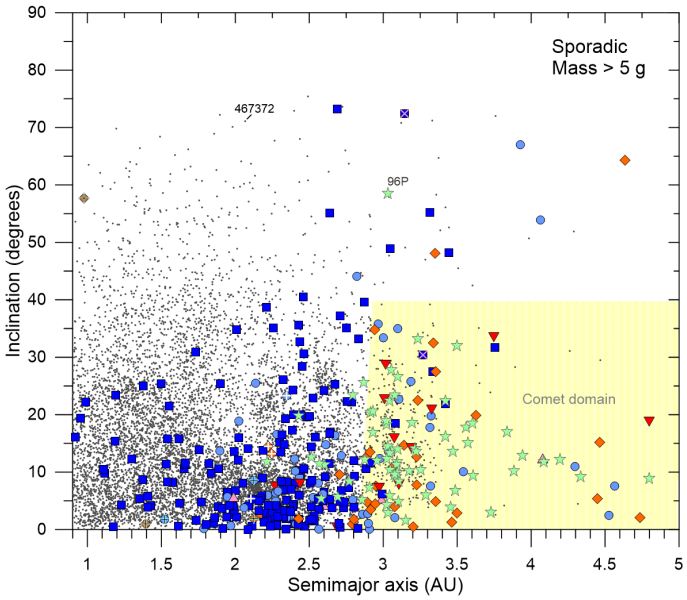

Fig. 9. Inclinations and semimajor axes of meteoroids of various Pf classes and near-Earth objects (asteroids and comets with perihelion distance $q < 1.3$ AU). Semimajor axes (a) are restricted to 0.9–5 AU. Only sporadic meteoroids (i.e., not belonging to any of the 16 major meteor showers) with masses larger than 5 g are shown. No meteoroid with $a < 5$ AU has inclination lager than 90°. Meteoroids with iron or Na-poor spectra are marked. See Fig. 8 for legends. The region occupied primarily by comets and cometary meteoroids is highlighted in yellow.

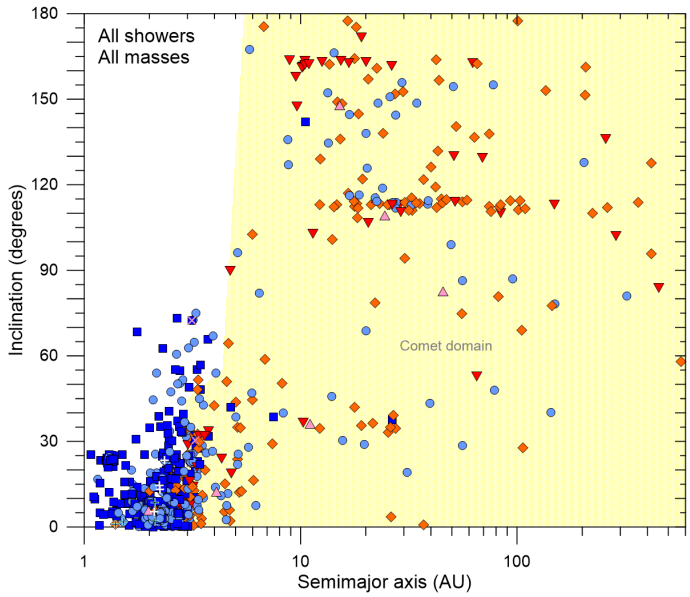

Fig. 10. Inclinations and semimajor axes of meteoroids of various Pf classes. Semimajor axes are shown up to 600 AU. Meteoroids with iron or Na-poor spectra are marked. See Fig. 8 for legends. The region occupied primarily by comets and cometary meteoroids is highlighted in yellow.

crosses in figures where confirmed irons are marked by black crosses. These suspected irons occupy the same orbital region and Pf range as the confirmed irons. Because of their sudden ends, irons are better separated from other asteroidal meteoroids using the P_E criterion than the Pf value.

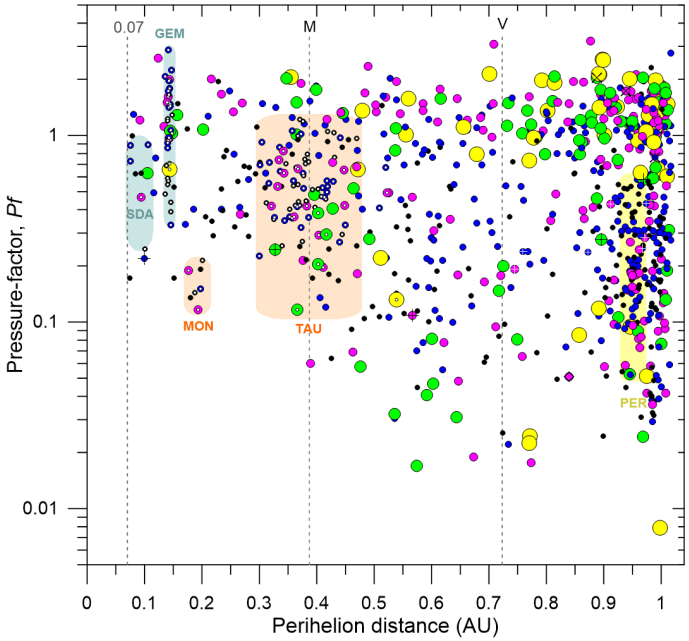

Fig. 11. Pressure factor as a function of perihelion distance. Meteoroid masses and spectra are marked as in Fig. 4. Vertical dashed lines indicate the semimajor axes of Venus, Mercury, and the distance of 0.07 AU. Regions where members of the Southern δ Aquariids, Geminids, December Monocerotids, Taurids and Perseids meteor showers are found are highlighted. Actual meteoroids belonging to the first four showers are marked by white dots.

Table 1. Fireballs without spectra suspected to be irons.

EN280817_233341	EN170418_194938
EN161017_185044	EN121118_185325
EN171017_205152	EN141118_195214
EN180318_001818	

There are 473 fireballs in our sample with aphelia less than 4.9 AU; 336 of them are sporadic (or belonging to minor showers). Probable irons represent 2.5% of all of them and nearly 3.6% of sporadic ones. The largest iron has a photometric mass of 0.25 kg, corresponding to a diameter of 4 cm. The iron fraction is probably higher among small asteroidal meteoroids (Mills et al. 2021).

3.5. Extreme orbits

In this section, we check how perihelion distance and orbital eccentricity relates to the physical classification of meteoroids. We also check the resonances with Jupiter.

3.5.1. Perihelion distances

Figure 11 shows Pf plotted against perihelion distance, q. All very susceptible meteoroids with $Pf < 0.1$ have perihelion distances higher than 0.35 AU. There are, nevertheless, some susceptible Pf-III meteoroids with $0.1 < Pf < 0.27$ even at $q < 0.2$ AU. Some of them belong to the December Monocerotid shower and are supposedly relatively young. Another one is an iron, and thus, in fact, a quite compact body. The others are small meteoroids. But most meteoroids with low perihelia are resistant. Those with masses larger than 100 g all have

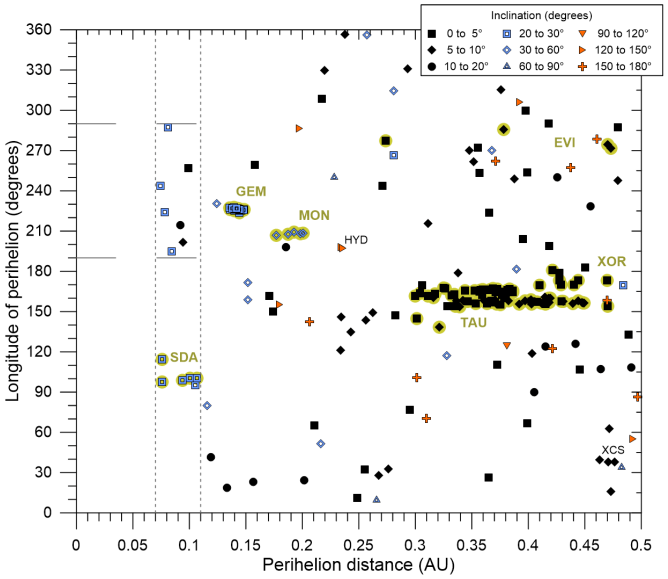

Fig. 12. Longitude of perihelion as a function of perihelion distance. Different symbols correspond to different inclination intervals (see the legend). Meteoroids belonging to major meteor showers (Southern δ Aquariids, Geminids, December Monocerotids, Taurids, η Virginids, and χ Orionids) are highlighted. Minor showers σ Hydrids (HYD) and ξ^2 Capricornids (XCS) are also marked. The excess of sporadic meteoroids with $q < 0.11$ AU at $190° < \tilde{\omega} < 290°$ is notable.

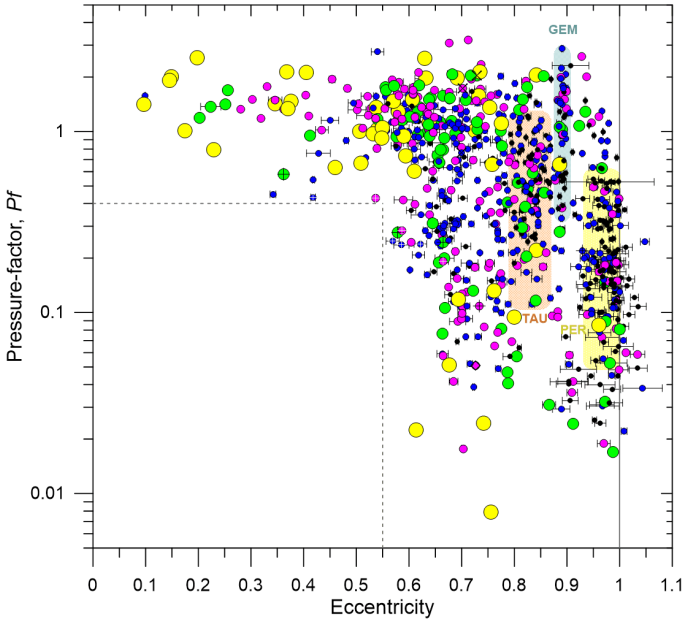

Fig. 13. Pressure factor as a function of eccentricity. Meteoroid masses and spectra are marked as in Fig. 4. Regions where members of the Taurids, Geminids, and Perseids meteor showers are found are highlighted. Formal error bars of eccentricities are included. The vertical solid line marks the parabolic limit. The dashed lines border the region with no meteoroids.

a $Pf > 0.6$. Many observed resistant low-perihelion bodies are Geminids, and some are Southern δ Aquariids, which have even lower q. However, no meteoroid was observed at $q < 0.07$ AU. This seems to be significant (see also the histogram of q in the Appendix of Paper I) and corresponds with the lack of asteroids with $q < 0.076$ AU (Granvik et al. 2016; Wiegert et al. 2020).

It is worth mentioning that the longitudes of perihelia, $\tilde{\omega}$, of all seven sporadic meteoroids with $q < 0.11$ AU, lie between 190° and 290° (Fig. 12). Wiegert et al. (2020) found the region $180° < \tilde{\omega} < 270°$ and $i < 12°$ to be least contaminated by small cometary meteoroids, which may serve as impactors destroying larger bodies. At higher inclinations, this region may be linked with Geminids. The only other meteoroids with very low perihelia are five Southern δ Aquariids and one Northern δ Aquariid, all concentrated at $95° < \tilde{\omega} < 115°$. At larger perihelion distances, especially $q > 0.2$ AU, longitudes of perihelia of sporadic meteoroids are more randomly distributed. We note that only five retrograde meteoroids have $q < 0.3$ AU, two of them belonging to the σ Hydrid shower.

In general, the largest concentration of perihelion distances is near 1 AU. Meteoroids in such orbits have the highest probability of collision with the Earth.

3.5.2. Eccentricities

Figure 13 shows Pf plotted against eccentricity, e. Only resistant meteoroids with $Pf > 0.4$ were observed at $e < 0.55$. These are typically asteroidal orbits (all of them are prograde). Semimajor axes are lower than 2.2 AU; otherwise Earth encounter would not occur. Mostly large meteoroids are encountered here. Because of low entry velocities, small meteoroids remain under the detection limit.

There are 15 fireballs with hyperbolic orbits within one sigma of the formal error. Only two remain hyperbolic within three sigma limits. The largest eccentricity, $e = 1.048 \pm 0.009$, was measured for EN271117_012837. This fireball was nicely observed at one station but the other two records are from a large distance. The error may therefore be underestimated. It is possible that the fireball was a member of the minor (and unconfirmed) December ϵ Craterids meteor shower. With $Pf = 0.25$, it had a medium resistance. The second good candidate is EN190918_213159 with $e = 1.028 \pm 0.008$. It was observed very well and had a cometary $Pf = 0.11$.

Although most of the hyperbolic orbits are probably the result of observational errors, it is possible that some of them were truly hyperbolic. Nevertheless, the eccentricity in all cases is only slightly above unity and there is no reason to consider the meteoroids to be of interstellar origin. Orbits that were originally highly eccentric elliptic orbits could be transformed to hyperbolic orbits by gravitational disturbances of planets, nongravitational forces, or during the ejection process from the parent body. All hyperbolic orbits, except one with $i = 59°$, are retrograde. Meteoroid masses range from subgram to about 20 g. All Pf values are below 0.4, so as expected, the bodies are of cometary nature, similar to or slightly weaker than those encountered among the Perseids.

3.5.3. Resonances

Figure 14 suggests that there may be a small excess of meteoroids in the 1:1 resonance with Jupiter near 5.2 AU. Figure 15 shows that these meteoroids have moderate inclinations between 10°–45°. Physical classification is consistent with a cometary origin. No meteoroids were detected here with $i < 10°$, despite the presence of comet 85P/Boethin here. A similar situation may be present in the 3:2 resonance near 4 AU. In contrast to the resonant regions, there are low-inclination meteoroids around 4.6 AU. Comet 85P probably broke apart (Meech et al. 2013).

At lower semimajor axes, there is no clear excess (or lack) of meteoroids in resonance with Jupiter (see Fig. 14), except

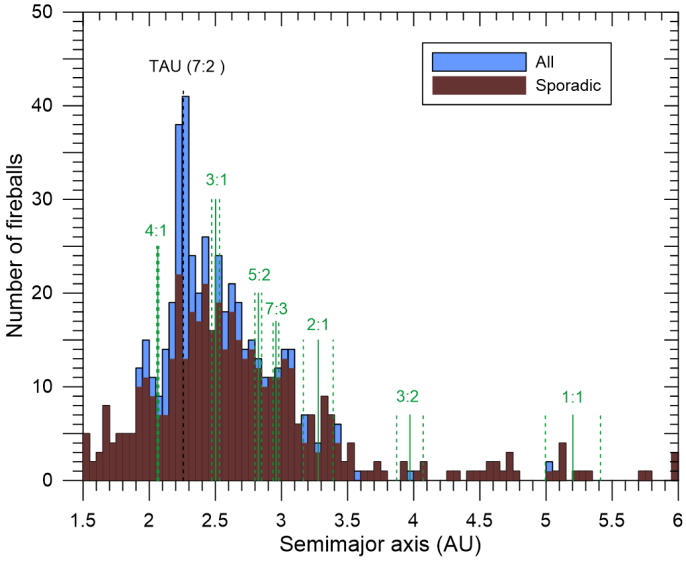

Fig. 14. Histograms of semimajor axes in the range 1.5–6 AU for all meteoroids and sporadic ones. The positions and widths of mean motion resonances with Jupiter (Tancredi 2014) are shown. The location of Taurids is indicated. The sporadic sample was created by removing members of the 16 major meteor showers.

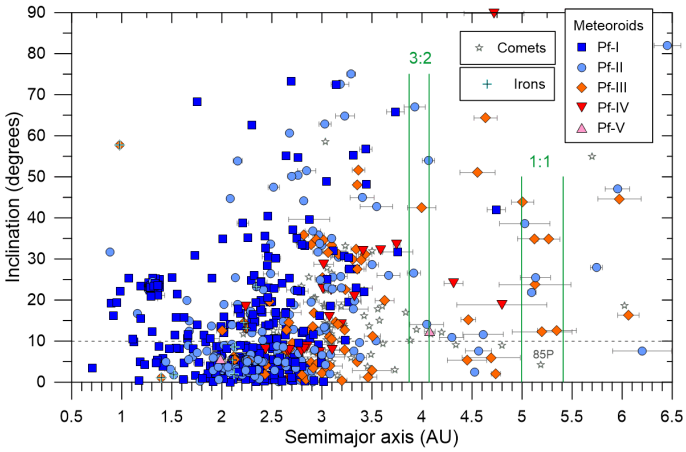

Fig. 15. Inclination as a function of semimajor axis in the range 0.5–6.5 AU. Meteoroids of various Pf classes and comets with perihelion distances $q < 1.3$ AU are shown. Probable iron meteoroids are marked. Error bars of semimajor axes are shown (errors in inclination are negligible at this scale). The intervals of semimajor axes corresponding to 1:1 and 3:2 resonances with Jupiter (Tancredi 2014) are indicated. No meteoroids with inclinations below 10° were detected inside these resonances. The same is valid for the 1:1 resonance with the Earth near 1 AU.

Taurids trapped in the 7:2 resonance (Spurný et al. 2017). However, it can be noted that no meteoroids with low inclination were detected near the 1:1 resonance with the Earth (Fig. 15).

4. Meteor showers

The major established meteor showers detected in our sample have been listed and the position of their radiants have been plotted in Paper I. The physical properties of the meteoroids of these showers have been discussed in Sect. 3.3. In this section, we first provide more details about the radiants and orbits of the most frequently detected showers, the Geminids, Perseids, and α Capricornids. Taurids have been already discussed by Spurný & Borovička (2019) and will be presented in more detail elsewhere. Then, we discuss the detection of minor showers, whether established or not.

4.1. Major showers

4.1.1. Geminids

Figure 16 shows the radiant coordinates and geocentric velocities of Geminids as a function of solar longitude. The data are compared with mean radiant positions and motions reported by other authors as cited in the International Astronomical Union Meteor Data Center (IAU MDC)[2] (Jopek & Kaňuchová 2017). We observed slightly larger right ascensions, although the reason for this is not clear. Other authors used various techniques (photographic, video, radar) sensitive to meteoroids with various masses and having various precisions. The declinations are in good agreement. As for velocities, the scatter of individual values in our data is lower than the range of mean values from other sources.

Figure 17 shows the radiant positions in a half-day interval during the shower maximum. Except for one outlier, the radiants are confined in an area of one degree in declination and one and a half degrees in right ascension. Ryabova (2021) computed the theoretical size and shape of radiant area under the assumption that 2000 yr ago, meteoroids were ejected from the parent body 3200 Phaethon by a cometary outgassing process. The computed area is somewhat smaller than one degree for milligram meteoroids and is expected to be smaller for larger bodies. Our radiants occupy a larger area, which may suggest that the ejection speeds were larger, or that the shower is older or was dispersed by some additional effects (e.g., nongravitational forces).

Our radiant is more compact than that reported by Moorhead et al. (2021) from video observations. Applying the methodology of subtracting radiant motion to all Geminds, we obtained a median deviation from the mean radiant of 0.29°, while Moorhead et al. (2021) found 0.38°. This either suggests that larger meteoroids are indeed less dispersed, or that our data are more precise. Kresák & Porubčan (1970) obtained 0.49° from old photographic data.

An interesting pattern is seen in Fig. 18, where eccentricity and inclination are plotted against the semimajor axis. There seems to be a core and a wing of the stream. The core has a semimajor axis similar to that of Phaethon and a somewhat lower eccentricity, and thus a larger perihelion distance than Phaethon (~ 0.145 AU vs. 0.140 AU). The wing extends from the core to larger semimajor axes and somewhat lower perihelion distances (but with a larger scatter). The core is rather extended in inclination, from that of Phaethon to about two degrees larger. The wing is more concentrated in inclination but with some outliers. Core and wing meteoroids are mixed in the stream, and meteoroids of both components are encountered throughout the duration of the shower. The core meteoroids are those with lower geocentric velocities (cf. Fig. 16c). Comparing the data with the computations of Ryabova (2022), we can see that the core consists of meteoroids of smaller masses in her model than the wing meteoroids. Her model, however, does not produce any Geminids with semimajor axes larger than 1.32 AU, while in reality the wing extends up to 1.375 AU.

[2] https://www.ta3.sk/IAUC22DB/MDC2007/, accessed November 22, 2021.

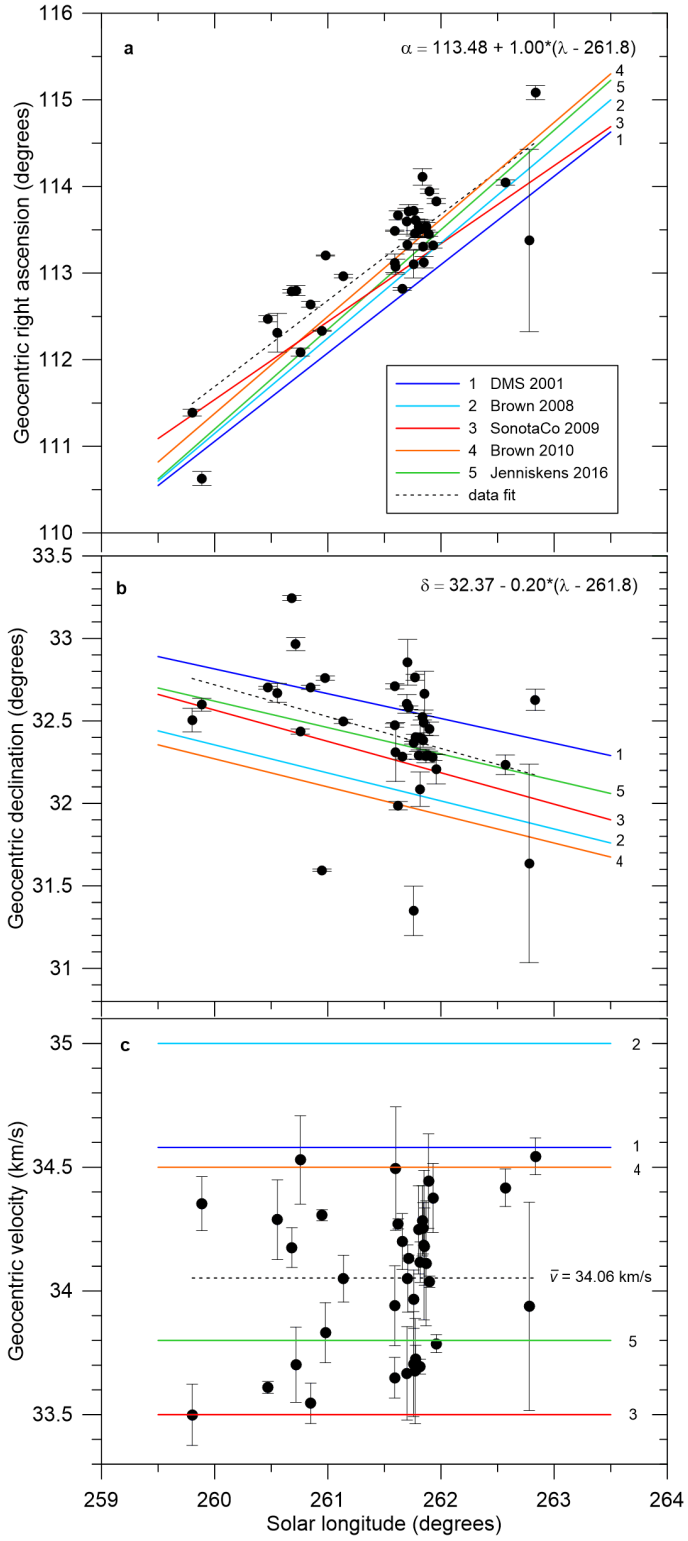

Fig. 16. Motion of the Geminid geocentric radiant. Right ascension (*panel a*), declination (*panel b*), and velocity (*panel c*) are plotted as a function of solar longitude (all in equinox J2000.0) for individual meteoroids with formal error bars. The data fit is plotted as a dotted line and the corresponding equation is inserted (no change of velocity with solar longitude was assumed). The motion of the mean radiant as reported by authors cited in the IAU Meteor Data Center is plotted by solid lines as follows: 1 – Dutch Meteor Society data (see Jopek et al. 2003); 2 – Brown et al. (2008a); 3 – SonotaCo (2009); 4 – Brown et al. (2010); 5 – Jenniskens et al. (2016a).

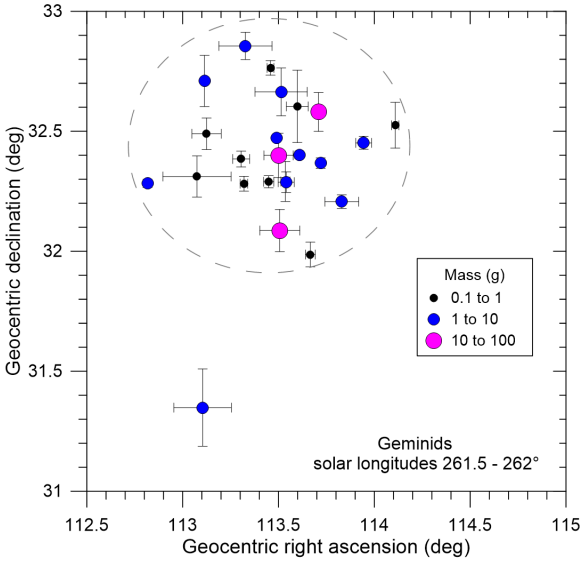

Fig. 17. Geminid radiants during the shower maximum (solar longitudes 261.5°–262.0°). Actual radiants, not corrected for radiant motion, are shown. Symbol sizes and colors distinguish three intervals of meteoroid masses.

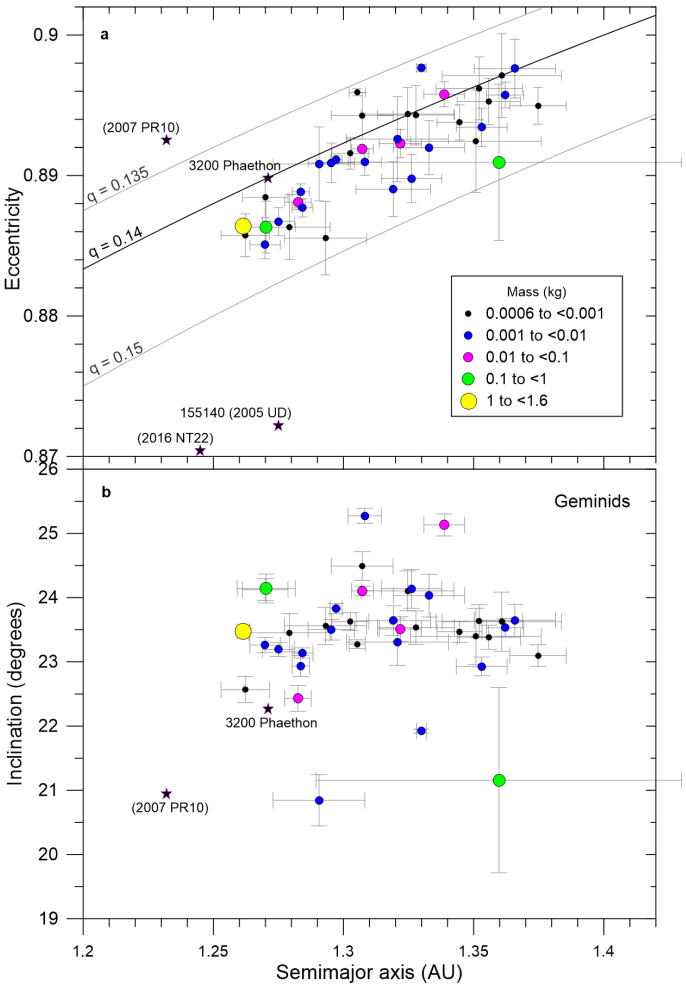

Fig. 18. Eccentricity (*a*) and inclination (*b*) as a function of semimajor axis for Geminid meteoroids. Lines of constant perihelion distance (in AU) are shown in *panel a*. Symbol sizes and colors distinguish five intervals of meteoroid masses. Four NEO asteroids fall in the *a*–*e* range of *panel a* and two of them have inclinations in the range of *panel (b)*.

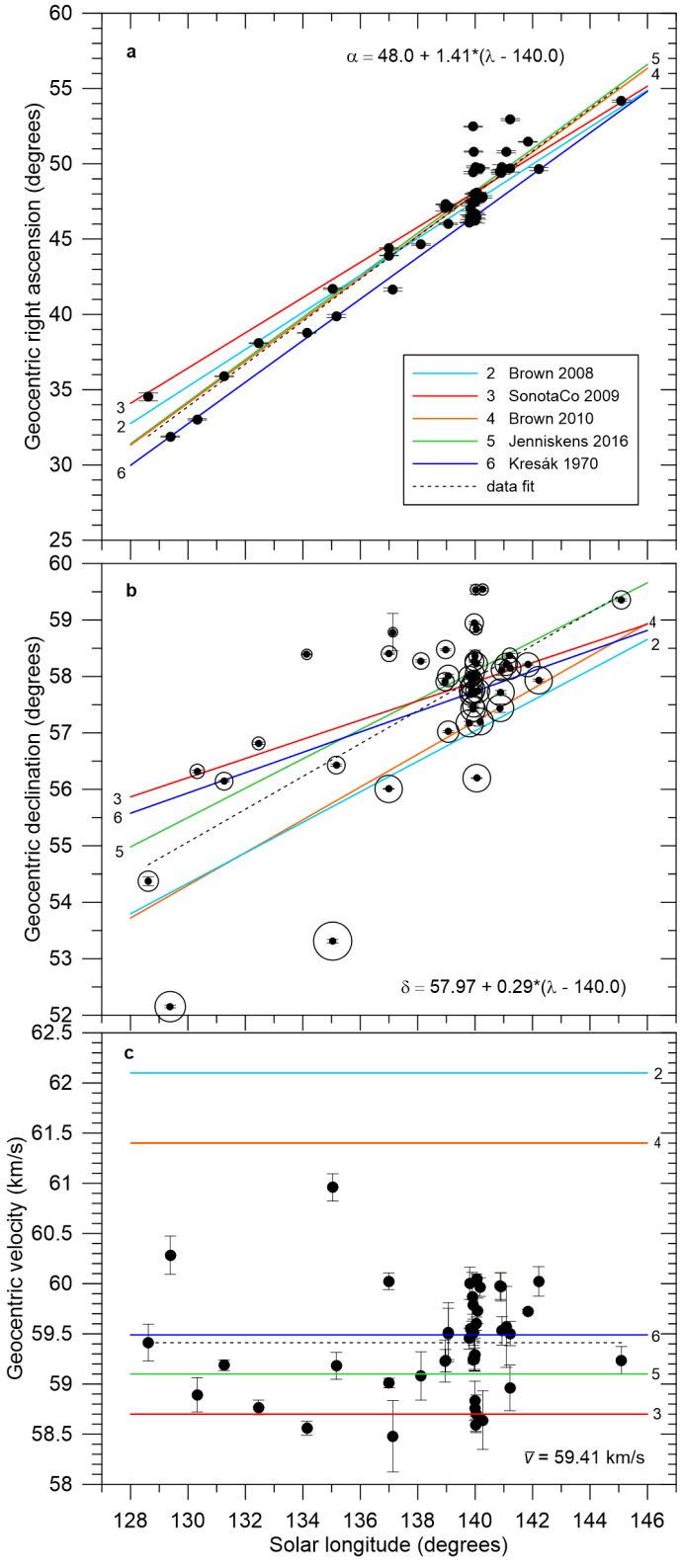

Fig. 19. Motion of the Perseid geocentric radiant. Right ascension (*panel a*), declination (*panel b*), and velocity (*panel c*) are plotted as a function of solar longitude (all in equinox J2000.0) for individual meteoroids with formal error bars. The sizes of the additional circles in plot *b* are proportional to velocity to show the correlation between declination and velocity. The data fit is plotted as a dotted line in all plots and the corresponding equation is inserted (no change of velocity with solar longitude was assumed). The motion of the mean radiant as reported by authors cited in the IAU Meteor Data Center is plotted by solid lines as follows: 2–5 see caption of Fig. 16; 6 – Kresák & Porubčan (1970).

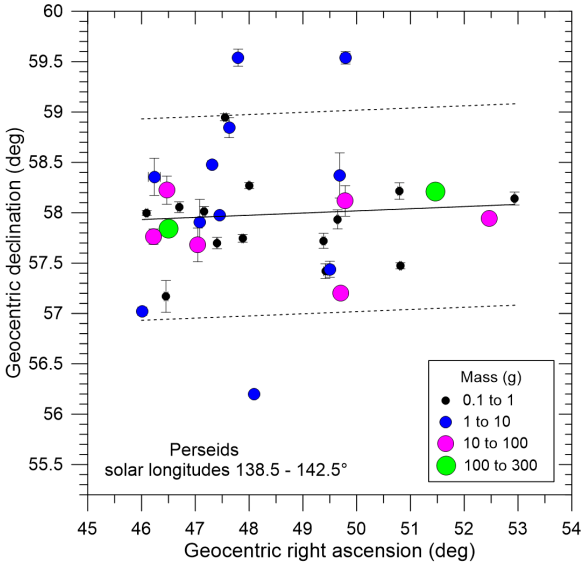

Fig. 20. Perseid radiants during four days of high activity of the shower (solar longitudes 138.5°–142.5°). Actual radiants, not corrected for radiant motion, are shown. Symbol sizes and colors distinguish four intervals of meteoroid masses. The solid line is a linear fit to the data. Dashed lines indicate the interval ±1° in declination around the fit.

4.1.2. Perseids

The radiant motion of Perseids (Fig. 19) in our data agrees with those of other authors, and most closely with that of Jenniskens et al. (2016a). The average geocentric velocity is closest to that of Kresák & Porubčan (1970). The velocities reported from radar (Brown et al. 2008a, 2010) are significantly higher. There is a clear correlation between velocity and declination of the radiant in our data (Fig. 19b): the lower the declination (in comparison with the value expected for the given solar longitude), the higher the velocity.

Figure 20 shows the radiant positions in a four-day interval during the shower maximum. Nearly 90% of radiants are confined to a band two degrees wide in declination. The extent in right ascension is partly due to radiant motion and is partly real (cf. Fig. 19a). If all Perseids are used and radiant motion is subtracted, the median deviation from the mean radiant is 0.88°. Moorhead et al. (2021) obtained 1.14° and Kresák & Porubčan (1970) reported 1.26°.

Individual eccentricities and semimajor axes are difficult to study for high-velocity meteors such as Perseids, because they are very sensitive to velocity determination. The average eccentricity of our 46 Perseid fireballs is 0.970 ± 0.003. The eccentricity of the parent comet 109P/Swift-Tuttle is 0.963. Therefore, the eccentricities and semimajor axes of meteoroids in our size range probably do not differ much from the parent comet. A similar result (e = 0.96) was obtained from 254 photographic Perseids by Kresák & Porubčan (1970) and from 4367 video Perseids by Jenniskens et al. (2016a), who listed e = 0.95. The value e = 0.896 reported recently from video data (10424 meteors) by Vida et al. (2021) is probably too small.

Perihelion distances and inclinations can be reliably computed for individual meteoroids and are plotted in Fig. 21 as a function of the longitude of ascending node (virtually equal to the solar longitude). Perihelion distances of most Perseids across the whole stream are between 0.945 and 0.965 AU, and are therefore similar to, or slightly lower than that of the parent comet (q = 0.9595 AU). Nevertheless, in the dense part of the stream

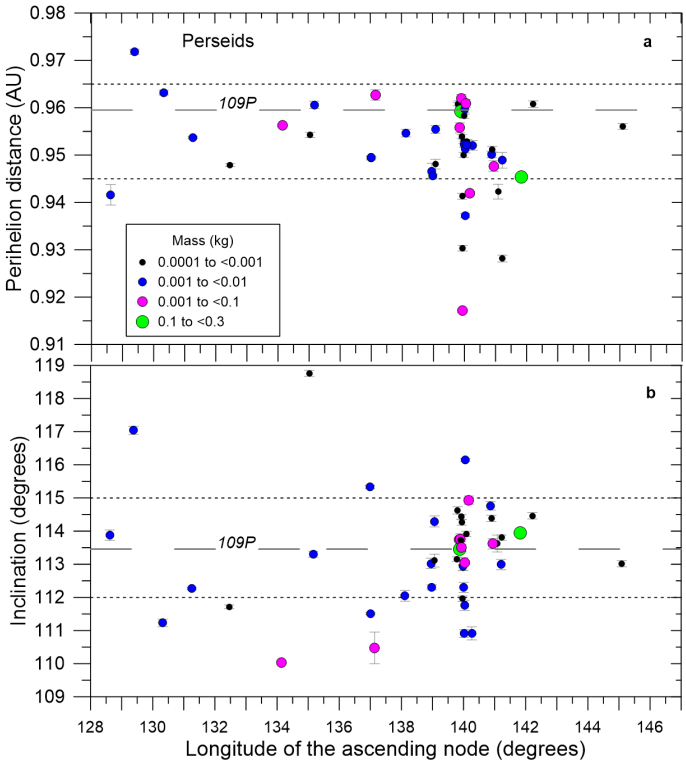

Fig. 21. Perihelion distance (*a*) and inclination (*b*) as a function of the longitude of ascending node for Perseid meteoroids. Symbol sizes and colors distinguish four intervals of meteoroid masses. The dashed gray lines show the values for the parent comet 109P/Swift-Tuttle. The dotted lines mark the intervals where most Perseids are confined.

around solar longitudes of 140°, about 20% of meteoroids have lower perihelion distances, down to 0.915 AU. They are those with the right ascension of the radiant larger than expected from the general trend (cf. Fig. 19a). Low-perihelion Perseids seem to be absent, or at least less numerous in the outer parts of the stream, although the statistics are rather poor there.

In contrast, orbital inclinations are concentrated around the inclination of the parent comet (i = 113.45°) in the dense part of the stream and are much more scattered at lower solar longitudes. Outlying inclinations correspond to outlying declinations of radiants (cf. Fig. 19b). The lowest inclination, 110.0°, had fireball EN060818_221424, which was observed very well and also had a high eccentricity, 0.995 ± 0.006. Our data suggest that meteoroids with lower inclinations have high eccentricities and that meteoroids with higher inclinations have lower eccentricities, but this cannot be proven because the uncertainties of eccentricities are too high in most cases.

4.1.3. α Capricornids

There are only ten α Capricornids in our sample but the radiant motion is well defined (Fig. 22). Our data for right ascension are closest to the drift proposed by Hasegawa (2001). The data for declination are in agreement with most authors cited in the IAU MDC. The velocities from single station video data (Molau & Rendtel 2009) and from the AMOR radar (Galligan & Baggaley 2002) seem to be too high. Our data suggest a slight decrease in geocentric velocity during the shower activity. A similar result was obtained by Moorhead et al. (2021).

Eight of the ten α Capricornids have semimajor axes between 2.55 and 2.7 AU, and eccentricities between 0.76 and 0.78,

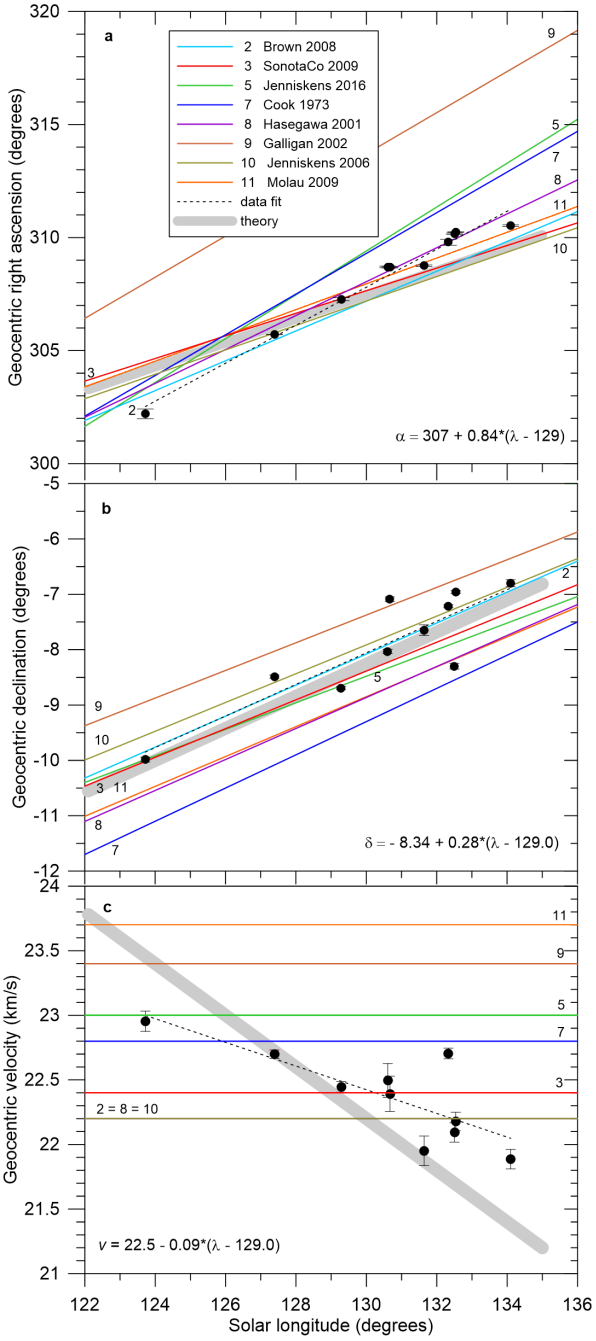

Fig. 22. Motion of the α Capricornid geocentric radiant. Right ascension (*panel a*), declination (*panel b*), and velocity (*panel c*) are plotted as a function of solar longitude (all in equinox J2000.0) for individual meteoroids with formal error bars. The data fit is plotted as a dotted line in all plots and the corresponding equation is inserted. The motion of the mean radiant as reported by authors cited in the IAU Meteor Data Center is plotted by solid lines as follows: 2, 3, 5 see caption of Fig. 16; 7 – Cook (1973); 8 – Hasegawa (2001); 9 – Galligan & Baggaley (2002); 10 – Jenniskens (2006); 11 – Molau & Rendtel (2009). The thick gray lines show the motion of theoretical radiants for particles ejected from comet 169P/NEAT between 2000 and 5000 yr ago (Jenniskens & Vaubaillon 2010).

corresponding to perihelion distances 0.59–0.62 AU (the other two have a similar q but $a \sim 2.8$ AU). These parameters perfectly match comet 169P/NEAT (see Fig. 8), which is likely the parent body of the stream (Jenniskens & Vaubaillon 2010). Comet P/2003 T12 (SOHO), also mentioned in connection with

α Capricornids (Jenniskens et al. 2016a), is not far in this respect. But the inclinations and other angular elements of both comets are different. Nevertheless, as shown by Jenniskens & Vaubaillon (2010), meteoroids released from 169P/NEAT between 2000 and 5000 yr ago could evolve into the current α Capricornid orbit. The modeled theoretical radiants match the observations; the velocity match is somewhat worse (Fig. 22).

More recently, it has been proposed that asteroid 2017 MB1 is associated with the stream (Wiegert et al. 2017; Ye 2018). The matches of the angular elements and the perihelion distance are good, but the semimajor axis of 2017 MB1 is only 2.374 AU. There are other, though smaller, asteroids with similarly good orbital matches: 2015 DA54, 2016 BN14, or 2019 CZ1. The latter two have short data-arc spans and rather uncertain orbits.

4.2. Minor showers

In addition to the 16 major and well-known meteor showers discussed so far in this paper, the associations of some fireballs with minor showers are provided in the catalog. These associations should be considered as a suggestion. In this section we discuss some of these associations, where at least three or a pair of closely related fireballs were detected. Established showers are discussed first, followed by showers on the working list (as of November 2021). The tables for this section are given in Appendix A.

4.3. Established minor showers

Five fireballs may be associated with either the Northern or Southern δ Cancrids (NCC and SCC, respectively). They are listed in Table A.1. Only the selected orbital elements without errors and the *Pf* value characterizing the physical properties of the meteoroids are given. Complete data can be found in the catalog. The δ Cancrids are a diffuse ecliptical shower overlapping with the antihelion source, and are therefore subject to sporadic contamination. None of our five fireballs can be firmly classified as a shower member. Three of them were observed within 6 h on January 20, 2017, and have mutually similar orbits, but these are somewhat different from the nominal orbit of δ Cancrids. The perihelion distance was larger. All of them had $Pf > 1$, and were therefore resistant bodies likely of asteroidal origin. Also, their orbits were asteroidal. It is possible that it was a random association.

Two fireballs were detected from the σ Hydrids (HYD), July γ Draconids (184 GDR), and κ Ursae Majorids (KUM). All these showers have long-period orbits, are well defined, and there is no doubt about the fireball shower membership (Table A.2). Our data suggest a larger eccentricity, and thus a longer orbital period of July γ Draconids than previously thought. Both σ Hydrids and July γ Draconids had $Pf \sim 0.4$, which ranks them among the most resistant meteoroids on Halley-type orbits. The *Pf* of κ Ursae Majorids was one order of magnitude smaller and they belong, on the contrary, to the weakest meteoroids.

Two fireballs were possibly detected also from the x Herculids (XHE) and one from each of 13 other established minor showers (AVB, NDA, TAH, COR, SSG, SZC, AUD, OCC, OCT, XUM, PPS, LUM, and SLD). The association with the shower is, however, uncertain in some cases.

4.4. Showers on the working list

Among the showers on the working list of the IAU MDC, the most associations were obtained for the ν Draconids (NDR). This toroidal shower has a dispersed radiant (Jenniskens et al. 2016b) and random associations are, therefore, possible. Five possible ν Draconids were identified (Table A.3). Meteoroid EN180918_030212 had high ablation resistance ($Pf = 1.4$) but also rather low eccentricity. Its aphelion was at 4.1 AU, while the aphelia of the other four meteoroids were at 4.9–5.7 AU. It is quite possible that EN180918_030212 did not belong to the ν Draconids. If so, the range of *Pf* of the ν Draconids was similar to the κ Cygnids.

Table A.4 provides a list of six fireballs detected over a period of one month but with radiants close together in the ecliptic coordinates related to the Sun (near $\lambda - \lambda_\odot = 198°$, $\beta = -5°$, see the plot in Paper I). Their perihelion distances are also similar, so the fireballs may be related. The associated showers may be Southern δ Piscids (SPI), Southern October δ Arietids (SOA), or ξ Arietids (XAR). These showers are probably also related and differ mainly by the period of activity. According to Jenniskens et al. (2016a), they may belong to the Encke Complex. The fireball orbits are distinct from those of the Southern Taurids by smaller perihelion distances and, except one, also by smaller semimajor axes. Inclinations are also slightly higher in most cases. Fireballs EN150918_231506 and EN131018_020534 may be random interlopers (their semimajor axes and inclinations differ from the other four fireballs) but the other four may belong to a single shower active at the end of September and in the first half of October. All four were small bodies with masses up to 1 g and their *Pf* was similar to those of Taurids of the same sizes, in other words relatively high.

Four fireballs could be associated with each of these showers on the working list: λ Ophiuchids (460 LOP), December ζ Taurids (638 DZT), and λ Leonids (733 LAL). All these proposed showers have indistinct orbits with low inclinations and a Tisserand parameters near three. Since there are many sporadic meteors with this type of orbit and the possibly associated fireballs are not clustered, we cannot confirm the detection of any of these showers. The situation is the same for two showers with three fireballs: June ϵ Ophiuchids (459 JEO) and February π Leonids (501 FPL). In fact, four associations were also detected for the April β Sextantids (449 ABS) and three for May α Comae Berenicids (455 MAC), which have both been removed from the working list and are now considered nonexistent. This demonstrates that most associations with these proposed ecliptical showers are probably random.

There is a somewhat different situation with the April ψ Ursae Majorids (133 PUM), with three possible fireballs. The orbits of the fireballs are quite different but there are also several different orbits of this shower listed in the IAU MDC. Different fireballs were therefore paired with orbits of different authors. Thus, the detection of this shower cannot be confirmed.

The detection of the toroidal shower August μ Draconids (AMD) is more probable. Three candidate fireballs are listed in Table A.5. The shower radiant is close to that of established showers κ Cygnids (KCG) and August Draconids (AUD), and all three showers may be related (Jenniskens et al. 2016a). Two fireballs had *Pf* values similar to κ Cygnids but EN260817_185317 was much more resistant. Since it also had a larger eccentricity, it may in fact not be a member of the shower.

The detection of ξ^2 Capricornids (XCS) is even better. Three candidate fireballs with quite similar radiants and orbits were detected within one degree of solar longitude (Table A.5). The shower may be related to α Capricornids and comet P/2003 T12 (SOHO; Jenniskens et al. 2016a). ξ^2 Capricornids have smaller perihelion distances and semimajor axes than α Capricornids. All three fireballs exhibited bright flares and the *Pf* values were

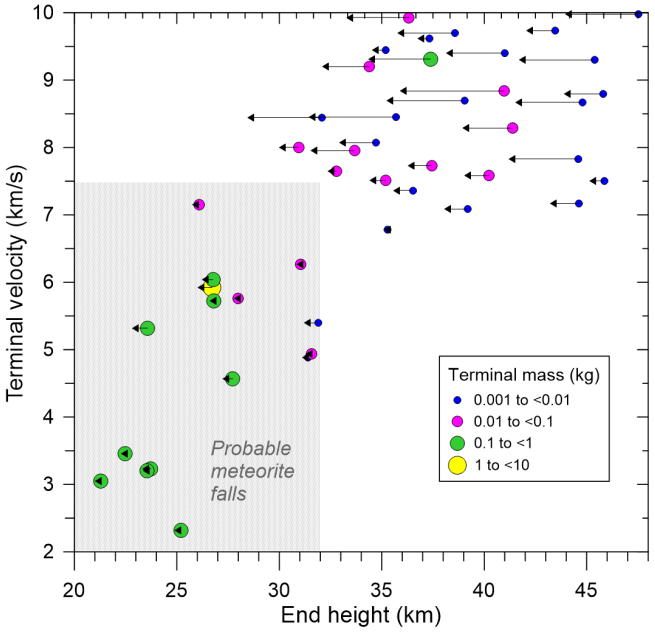

Fig. 23. Terminal velocities and end heights for fireballs with computed terminal masses larger than 1 g. The terminal mass is coded by the symbol size and color. The symbols are placed at the heights where terminal velocities were measured. The arrows point to the actual end heights, which are lower in cases where velocity was difficult to measure toward the fireball end. The velocity at the end is expected to be lower than shown in these cases. The shaded area encompass fireballs with a high probability of dropping a meteorite larger than 1 g.

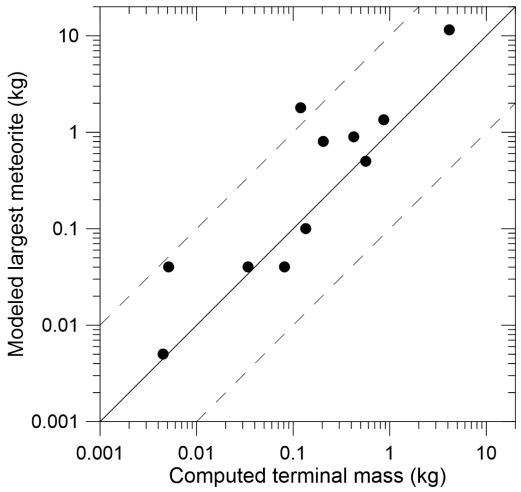

Fig. 24. Comparison of terminal masses from the present catalog with the mass of the largest expected meteorite resulting from fragmentation modeling by Borovička et al. (2020) for 11 fireballs. The solid line marks equality of both approaches and the dashed lines mark an order of magnitude difference.

similarly low as for α Capricornids. The photometric masses ranged from 30 g to almost a kilogram. Other showers from the working list have, at most, two possible detections.

5. Terminal masses and meteorite falls

One of the purposes of fireball networks is the recovery of meteorites. In 2017–2018, the European Fireball Network recovered one meteorite – Renchen (Spurný et al. 2019; Bischoff et al. 2019). That fireball and meteorite fall occurred in western Germany near the French border. It was captured by two digital cameras close to the horizon but the velocity could be measured only on the cameras of the German part of the network. The fireball is therefore not included in this catalog. A paper devoted to the Renchen fall will be published elsewhere.

The catalog contains terminal masses indicating a possibility of meteorite fall. However, the masses are only approximate and result from the four-parameter velocity fitting of the whole fireball, ignoring any fragmentation. Terminal masses are listed only if they are larger than 1 g and if the terminal velocity is lower than 10 km s^{-1}.

Figure 23 shows the end heights and terminal velocities for fireballs with nonzero terminal masses. In some cases, the terminal velocity could not be measured at the end height because the shutter breaks were either faint and noisy, or not well separated. Therefore, both the height of the last velocity measurement and the end height are plotted. The measured terminal velocity is given, while the terminal mass is computed for the end height as a result of extrapolation of the four-parameter fit.

We can see that there are many fireballs with terminal velocities above 7 km s^{-1} measured at heights above 30 km. Terminal masses are below 0.1 kg, except for one case where the terminal mass is slightly above this value (0.13 kg for EN071118_010142). Since ablation continues down to ~ 3 km s^{-1}, it can be expected that most of these fireballs did not drop any significant meteorite. In an exceptional case, that of EN071118_010142 over northern Poland, the relatively high end height and terminal mass may have been caused by the large distance to the fireball, and a non-negligible meteorite fall cannot be excluded.

The much more likely meteorite falls are those with end heights below 32 km and terminal velocities below 7.5 km s^{-1}. This area is shaded in Fig. 23 and contains 16 fireballs. Eleven of them have been included in the fragmentation modeling of Borovička et al. (2020). Fragmentation modeling provides more reliable estimates of meteorite masses by considering the fragmentation points and fitting the dynamics from the last fragmentation toward the end point. Figure 24 shows that the fragmentation model expects a larger meteorite than the routine procedure in most cases, and even by an order of magnitude in two cases. Nevertheless, even the result of fragmentation modeling is just an estimate. Not only does the mass depend on the assumed meteorite density and shape, but the meteorites sometimes break-up further during the dark flight, as evidenced by incomplete coverage by the fusion crust (see e.g., Bischoff et al. 2019). We note that the mass of the largest meteorite is discussed here but in many cases the fall also includes numerous small meteorites, and it may be more likely to find some of them (see e.g., Spurný et al. 2020). Searches of various intensities were performed for ten meteorite falls discussed here, without success.

Satisfying the conditions $h_e < 32$ km and $v_e < 7.5$ km s^{-1}, though stricter than that of Halliday et al. (1989a) who gave rough limits 35 km and 10 km s^{-1}, cannot be considered as sufficient for a meteorite fall. It is necessary to evaluate also the deceleration and light curve. Nevertheless, all 16 fireballs from the present sample seem to be good candidates for dropping meteorites (although quite small meteorites in some cases). It is therefore worthwhile to take them as a special class of fireballs – likely meteorite droppers – and evaluate their orbits and pressure factors. Their geographic distribution is shown in Fig. 25, together with the less promising candidates.

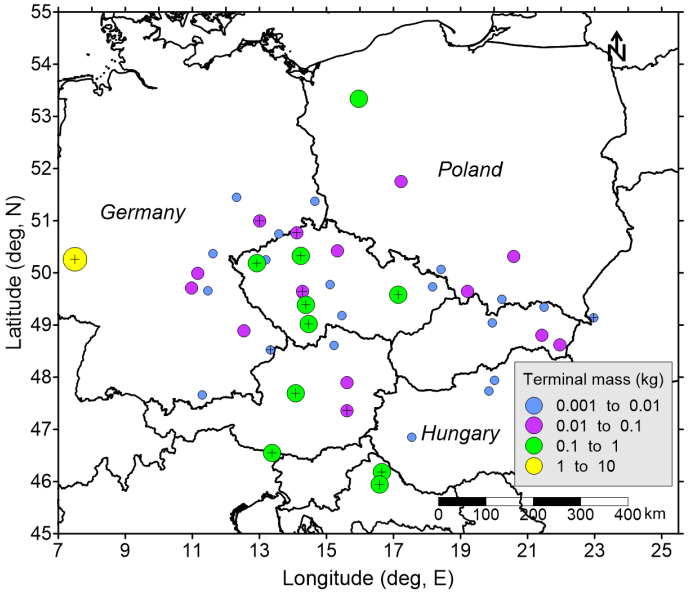

Fig. 25. Geographic distribution of fireballs with computed nonzero terminal masses. Those fireballs that probably ended with meteorite falls are marked by a cross. Most of the others probably ablated out after the last velocity measurement. The plotted positions are for the fireball end.

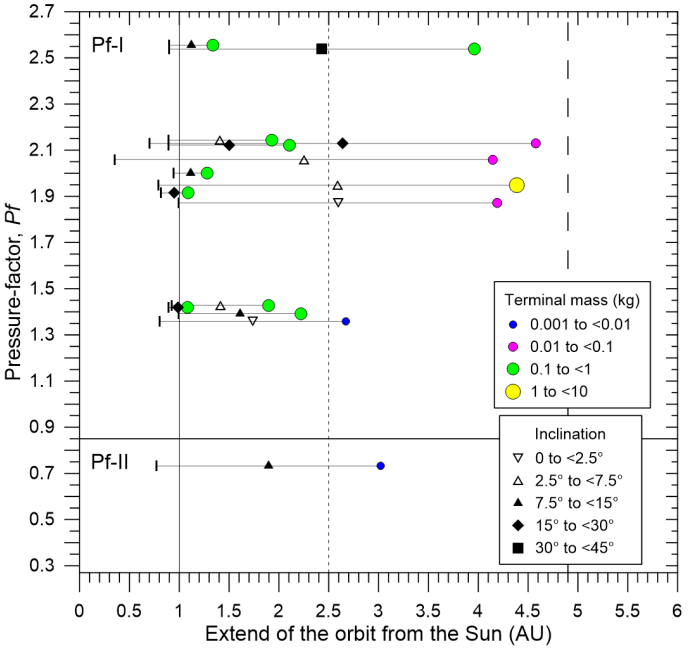

Fig. 26. Pressure factors (vertical axis) and sizes of the orbits (horizontal axis) for 15 probable meteorite falls. Each fireball is characterized by three symbols connected with a horizontal line. The vertical bar is plotted at the perihelion distance (q), a symbol encoding the orbital inclination (i) is plotted at the semimajor axis (a), and a colored circle encoding the terminal mass computed from the whole-trajectory fit is plotted at the aphelion distance (Q). Vertical lines indicate the Earth orbit (1 AU), 3:1 resonance with Jupiter (2.5 AU), and the limit for asteroidal orbits according to this paper (4.9 AU). The horizontal line indicates the boundary between the Pf-I and Pf-II classes (0.85). Fireball EN311018_161746 could not be included since it was observed during twilight and has no photometry or Pf. The orbital parameters are q = 0.925 AU, a = 2.45 AU, Q = 3.98 AU, and i = 8.6°.

The most important orbital parameters and Pf values of meteorite droppers are shown in Fig. 26[3]. Not surprisingly, all orbits are asteroidal with aphelia $Q < 4.9$ AU and low to moderate inclinations (up to 35°). Two were on Aten-type orbits with low eccentricities and inclinations about 20°. As expected, the pressure factors were mostly high, between 1.3 and 2.6. Only fireball EN160517_205435 had Pf=0.7. It was probably a carbonaceous body according to Borovička et al. (2020) and the modeling showed that it dropped only a few gram-sized meteorites.

We can also roughly evaluate meteorite fall statistics. Halliday et al. (1989b) concluded, on the basis of the observation of the Canadian Meteorite Observation and Recovery Project (MORP), that there are about nine meteorite falls per 10^6 km^2 per year with a total fallen mass larger than 1 kg, and 58 falls dropping more than 0.1 kg. We detected 12 fireballs in 2 yr with the computed mass of the main meteorite larger than 0.05 kg. The total fallen mass can be reasonably expected to exceed 0.1 kg in these cases. Our covered area is 7×10^5 km^2. Due to weather limitations, cameras exposed 40–60% of the prescribed dark time at different stations (52% on average). The covered fraction of the total time (day+night) was 18–26%. Since this time also includes the times when the skies were mostly cloudy and cameras were running, we use the lower limit. It gives us 48 meteorite falls per 10^6 km^2 per year, in reasonable agreement with Halliday et al. (1989b).

There were six fireballs with main mass exceeding 0.5 kg (see Fig. 24), with the total fallen mass thus probably exceeding 1 kg. It gives a rate about two times that of Halliday et al. (1989b) even when we take into account the fact that these brighter events can also be observed in poor conditions. But here we enter low number statistics and it seems that the covered years were somewhat richer in larger meteorite falls than average years.

6. Possible related asteroids

Some of the major meteor showers, such as the Perseids, Geminids, Leonids, or Lyrids, have well known parent bodies with orbits similar to the orbits of the meteors. They do not need to be discussed here. The situation may be more complicated for some other showers. The Taurids are a good example. Their parent body is most likely comet 2P/Encke. Spurný et al. (2017) have, nevertheless, identified several asteroids, most notably 2015 TX24, with orbits more similar to the resonant branch of the Southern Taurids. These asteroids can be considered as large members of the stream rather than parent bodies. Egal et al. (2021) confirm their orbital convergence with 2P/Encke and also with 2004 TG10, which is now related to the Northern Taurids, about 5000 yr ago. Here we note the close orbital similarity of another asteroid, 2014 NK52, with the Northern Taurids, namely with those observed around mid-November (while the orbit of 2004 TG10 is more similar to NTA meteors observed earlier in November). 2014 NK52 was not included in the work of Egal et al. (2021). That work did include 2003 WP21, which shows orbital similarity with the Southern Taurids observed by us toward the end of November, but orbital convergence with 2P/Encke was not found in this case.

[3] The orbits of EN141117_164658, EN080418_184736, and EN230518_194647 have been slightly changed in the catalog in comparison with those published in Borovička et al. (2020) since the method of computing velocities from supplementary video cameras has been improved.

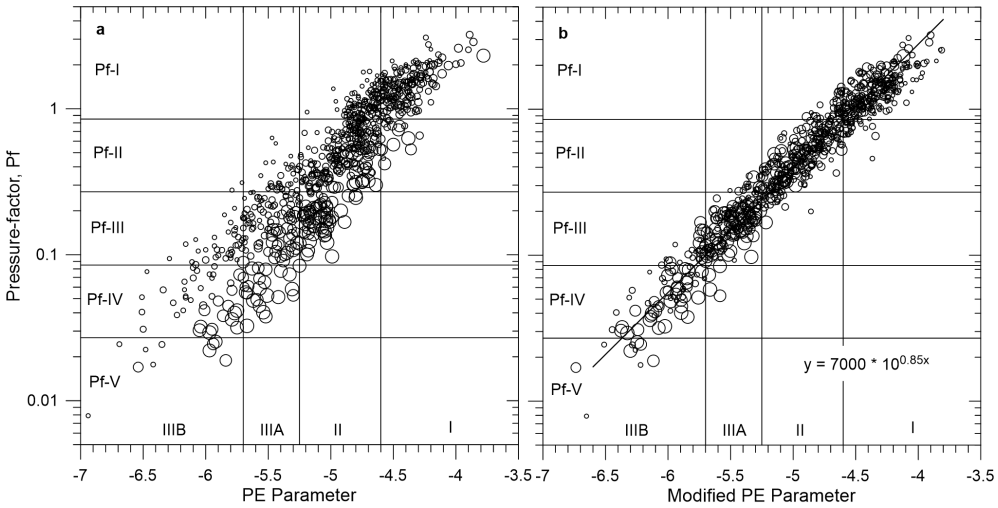

Fig. 27. Relation between the P_E and Pf parameters for all fireballs (*panel a*). The symbol size is proportional to fireball initial velocity. *Panel b* shows the same relation for the P_E parameter modified according to Eq. (4). A simple function is drawn through the data.

A situation similar to the Taurids is encountered in α Capricornids. Several asteroids, discussed in Sect. 4.1.3, have more similar orbits to the fireballs than the likely parent comet 169P/NEAT. The parent comets of both showers, 2P/Encke and 169P/NEAT, have orbits classified as asteroidal (see Fig. 8). The physical properties of Taurid and α Capricornid meteoroids are, nevertheless, different (see Sect. 3.3).

The orbits of two of the three observed August μ Draconids (Table A.5) were found to be close to the orbit of asteroid 2002 GJ8. That asteroid is on unstable cometary orbit (Fernández et al. 2014) and has a low albedo of 0.018 (Trilling et al. 2017)[4]. It was discussed in connection with κ Cygnids and related showers by Shiba (2017). As he noted, the current orbit was quite different before the encounter with Jupiter in 2015. Thus, the current orbital similarity with August μ Draconids is probably due to chance.

Asteroid 2003 AA83 has been associated with three fireballs (EN200117_181106, EN200117_192130, EN230117_202629). Two of them are possible δ Cancrids, but the orbital similarity is not particularly high. Moreover, asteroid 2003 AA83 was observed for only 6 days and its orbit is uncertain.

An additional run was done at the beginning of 2022, comparing the orbits of all known NEAs with sporadic fireballs on asteroidal orbits. The only asteroid having $D_{SH} < 0.05$ with three or more fireballs, where D_{SH} is the dissimilarity criterion of Southworth & Hawkins (1963), was found to be 2019 DN. The only asteroid with two associated fireballs was 2020 GV1. The comparison of the orbits for 2019 DN with the three fireballs is provided in Table A.6. Given that the fireball appearances span almost the whole month of March, this also is probably a chance coincidence. For two of the fireballs, asteroids with orbits even more similar than the orbit of 2019 DN exist.

We can conclude that, except for the Taurids and α Capricornids (and the well-known cases of Geminids), we have not found any convincing orbital similarity between multiple fireballs observed in 2017–2018 and asteroids. It does not mean that some individual links cannot exist.

[4] Data acquired from http://nearearthobjects.nau.edu/spitzerneos.html on January 6, 2022.

7. Discussion

7.1. The pressure factor, Pf

We have proposed a new one-dimensional metric to characterize meteoroid physical properties, which seems to be better than the P_E criterion of Ceplecha & McCrosky (1976). It is based on the maximal dynamic pressure encountered along the meteoroid trajectory, and we therefore called it the pressure resistance factor, or pressure factor for short, and abbreviated it as Pf. Provided that the fireball velocity could be measured along most of the trajectory, dynamic pressure is less dependent on observing conditions than the end height, which is the basis of the P_E criterion. Both metrics take into account meteoroid initial mass, velocity, and trajectory slope (in the case of P_E, unrealistically high initial mass resulting from the use of historical values of luminous efficiency must be entered). Both also need the knowledge of atmospheric density as a function of height.

Figure 27a compares the values of P_E and Pf for our sample of fireballs. The main difference turns out to be the velocity dependence. If the P_E is modified as follows:

$$P_E(\text{modified}) = P_E - \log v_\infty + 1.5, \quad (4)$$

(v_∞ is in km s^{-1}), much better correspondence between the two metrics is achieved (Fig. 27b). The remaining differences can be ascribed to the difference between considering end height and maximum dynamic pressure. For example, the modified P_E ascribes very high strength ($P_E \gtrsim -4$) to some very slow fireballs while Pf does not reach any extreme values ($Pf \lesssim 2$).

The pressure factor definition (Eq. (2)) was found empirically using the present sample of fireballs, which covers meteoroid masses from about 10^{-4} to 10^2 kg. In order to see if Pf values are reasonable for much larger meteoroids, we computed them in Table 2 for some more massive meteorite falls and very bright fireballs (superbolides) that disintegrated in the atmosphere completely. The input data including dynamic pressures were compiled from the literature. Velocities and trajectory slopes are well known in all cases, but dynamic pressures and especially meteoroid masses may be less certain.

The fireballs are divided into four groups according to meteorite type. Within the group, they are sorted according to initial

Table 2. Pressure factors, *Pf*, for bright meteorite-dropping fireballs and superbolides without meteorites.

Fireball	Meteorite type or Bolide date	m_∞ (kg)	v_∞ (km s^{-1})	p_{max} (MPa)	z (°)	*Pf*	References
	Ordinary and enstatite chondrites						
Chelyabinsk	LL5	1.2×10^7	19	18	72	0.31	[1]
Košice	H5	3500	15	6	30	0.78	[2]
Morávka	H5	1500	22.5	5	70	1.2	[3,4]
Neuschwanstein	EL6	300	21.0	9.6	40	2.0	[5,6]
Hamburg	H4	200	15.8	7	66	4.7	[7]
Žďár nad Sázavou	L3.9	150	21.9	2.7	65	1.2	[8]
	Mixed breccias						
Almahata Sitta	Ureilite+E+H+..	50,000	12.8	1.3	70	0.23	[9,10,6]
Benešov	LL3.5+H5+..	3500	21.3	9	9	0.61	[11,12]
	Carbonaceous chondrites						
Tagish Lake	C2	90,000	15.8	2.2	72	0.25	[13,6]
Flensburg	C1	20,000	19.4	2	65	0.20	[14]
Maribo	CM2	2000	28.3	5	59	0.5	[15]
	Large fragile bodies without meteorites						
Šumava	1974-12-04	5000	26.9	0.14	63	0.013	[16]
Romanian	2015-01-07	4500	27.8	3	47	0.18	[17]
Taurid	2015-10-31	650	33.1	0.19	78	0.055	[18,19]

References. [1] Borovička et al. (2013a), [2] Borovička et al. (2013b), [3] Borovička et al. (2003), [4] Borovička & Kalenda (2003), [5] Spurný et al. (2003), [6] Popova et al. (2011), [7] Brown et al. (2019), [8] Spurný et al. (2020), [9] Shaddad et al. (2010), [10] Borovička & Charvát (2009), [11] Spurný et al. (2014), [12] Borovička et al. (1998), [13] Hildebrand et al. (2006), [14] Borovička et al. (2019b), [15] Borovička et al. (2021), [16] Borovička & Spurný (1996), [17] Borovička et al. (2017), [18] Spurný et al. (2017), [19] Borovička & Spurný (2020).

mass. For ordinary and enstatite chondrites, we expect $Pf > 0.85$ corresponding to class Pf-I. It is so for most of them but not for Chelyabinsk, by far the largest body of all. It is reasonable to expect that above a certain mass limit, the maximum dynamic pressure does not depend, or depends only weakly, on mass. Thus, the pressure factor cannot be used for the classification of Chelyabinsk class bodies (diameter >10 m). The *Pf* is also somewhat lower than expected for Košice. This meteoroid larger than 1 meter fragmented heavily in the atmosphere (Borovička et al. 2013b), so the lower *Pf* can be ascribed to many internal cracks. On the contrary, an unusually large $Pf = 4.7$ was obtained for Hamburg. In this case, flares indicating fragmentation were observed only deep in the atmosphere (below heights of 26.5 km, see Brown et al. 2019). It seems that Hamburg was indeed a quite resistant meteoroid. Still, it is also possible that its initial mass was underestimated. We estimated the *Pf* also for the Carancas crater forming event, considered to be caused by an unusually strong meteoroid (see e.g., Brown et al. 2008b). Two sets of possible entry parameters from Borovička & Spurný (2008) were used: [1500 kg, 15 km s^{-1}, 16 MPa, 0°] and [10 000 kg, 20 km s^{-1}, 40 MPa, 30°]. In both cases, the result was $Pf = 2.4$, which is not an extreme value. Nevertheless, the lack of observations makes the Carancas data uncertain.

Next there are two mixed breccias, namely meteorite falls that produced meteorites of various types. The corresponding meteoroids were probably formed by the accumulation of fragments of several parent asteroids and can be expected to be less coherent than single-type meteoroids. Their *Pf* was indeed lower than those of ordinary chondrites. In the case of Almahata Sitta, it was near the boundary of the Pf-III and Pf-II classes, which may be connected with the fact that this body was composed mainly from ureilites, which are achondrites with a lower density than ordinary chondrites. Shaddad et al. (2010) classified the body as "cometary" of type IIIA/B but the Pf-classification does not point to such a low resistance.

For carbonaceous chondrites, we expect a *Pf* between 0.27 and 0.85, corresponding to the class Pf-II. It was so for Maribo. For Tagish Lake and Flensburg, both quite massive bodies, the *Pf* was somewhat lower. The reason for this may be that either the *Pf* is underestimated for large bodies or that large bodies are indeed composed of weaker material than smaller bodies of the same origin, as has been observed for some meteor showers (see Sect. 3.3).

Finally, there are three large meteoroid entries not accompanied with meteorite falls. The Romanian superbolide (Borovička et al. 2017) was caused by a relatively homogeneous body that disintegrated completely at dynamic pressures 1–3 MPa. The corresponding *Pf* is somewhat lower than for carbonaceous chondrites, which is what may be expected. The brightest Taurid EN311015_180520 observed by Spurný et al. (2017) in 2015 falls into the Pf-IV class, which corresponds with the Taurid trend of decreasing strength with increasing size. The internal structure of this meteoroid was investigated by Borovička & Spurný (2020). The 1974 Šumava superbolide was caused by one of the most fragile meteoroids ever observed and falls into the class Pf-V. It belonged to the Northern χ Orionids, part of the Taurid complex. We note that no massive meteoroids (>100 kg) have been observed on Halley-type orbits so far.

In summary, we conclude that the pressure factor *Pf* provides a reasonable quick classification of meteoroid physical properties for stony and cometary meteoroids of masses from 0.1 g up to about 10^5 kg. As is also the case for the P_E parameter, iron meteoroids cannot be identified using *Pf* only. Additional information, ideally the spectrum, is needed.

7.2. Physical properties of meteoroids from various sources

It is not a new result, but the *Pf* classification confirms that physical properties vary among meteoroids of common origin. The *Pf* values span an order of magnitude for all four of the best represented meteor showers in our sample (Taurids, Geminids, Perseids, and α Capricornids). This reflects the heterogeneity of their parent bodies. Still, we can observe clear differences between the showers. In Taurids, there is a pronounced trend of decreasing compactness with increasing size of the meteoroid. If we accept that the Šumava meteoroid was Taurid-related, the whole range from meter-sized extremely fragile bodies (probably porous dustballs) to centimeter-sized compact objects (stony projectiles) can be observed within that stream. A similar mass trend may be present in the Perseids and α Capricornids, but centimeter-sized meteoroids are less compact in these streams than in the Taurids and much larger meteoroids were not observed. In the Geminids, the mass trend is not present and although there is some overlap with Taurids, they generally contain more compact, probably denser, meteoroids.

Keeping in mind that neither asteroids nor comets are homogeneous bodies, we can still see differences between the physical properties of sporadic meteoroids in asteroidal and cometary orbits. In fact, the classification of physical properties allowed us to define approximate boundaries between asteroidal and cometary orbital domains. The domains are discussed in more detail in the following subsections.

7.2.1. Classical asteroidal orbits, $Q < 4.9$ AU

We have found that the aphelion distance, Q, is a better discriminator between asteroidal and cometary material than the Tisserand parameter, T. Most meteoroids with $Q < 4.9$ AU have asteroidal properties, although a significant fraction of them have $T < 3$ because they have either high eccentricity or high inclination. Thus, we defined classical asteroidal orbits as those having $Q < 4.9$ AU. Since their orbits must intersect the Earth's orbit, they have semimajor axes $a < 3$ AU. In our sample, all these orbits were prograde with inclination $i < 75°$. Of course, retrograde orbits could not be called classical asteroidal. Kresák (1969a) used a similar criterion: $Q < 4.6$ AU.

The histogram of *Pf* values for meteoroids on classical asteroidal orbits, excluding Taurids, Capricornids (α and ξ^2), and irons (known or suspected), is shown in Fig. 28a. Taurids and most Capricornids have classical asteroidal orbits, as have their parent comets. This situation can be considered as the intrusion of cometary bodies into the asteroidal domain. They were therefore removed from the sample, together with irons, to see the properties of other meteoroids on classical asteroidal orbits. As is shown in Fig. 28a, the majority of them indeed belong to the most resistant class Pf-I. A significant fraction also fall into the class Pf-II, especially the part with higher *Pf* values. We suppose that most of them are less resistant asteroidal meteoroids such as carbonaceous chondrites, but a contribution from comets is possible. Interestingly, there is a long tail of weaker bodies down to the most susceptible class Pf-V. They are almost certainly of cometary origin.

The histogram for Taurids and Capricornids (dominated by Taurids) is in Fig. 28c. The majority is of class Pf-II. The larger bodies in particular tend to be weaker and belong to Pf-III or Pf-IV. On the other hand, some small meteoroids enter the Pf-I region.

Irons, as already discussed, cannot be well classified using the *Pf* value. Formally, they fall into the Pf-III or the Pf-II class (Fig. 28e).

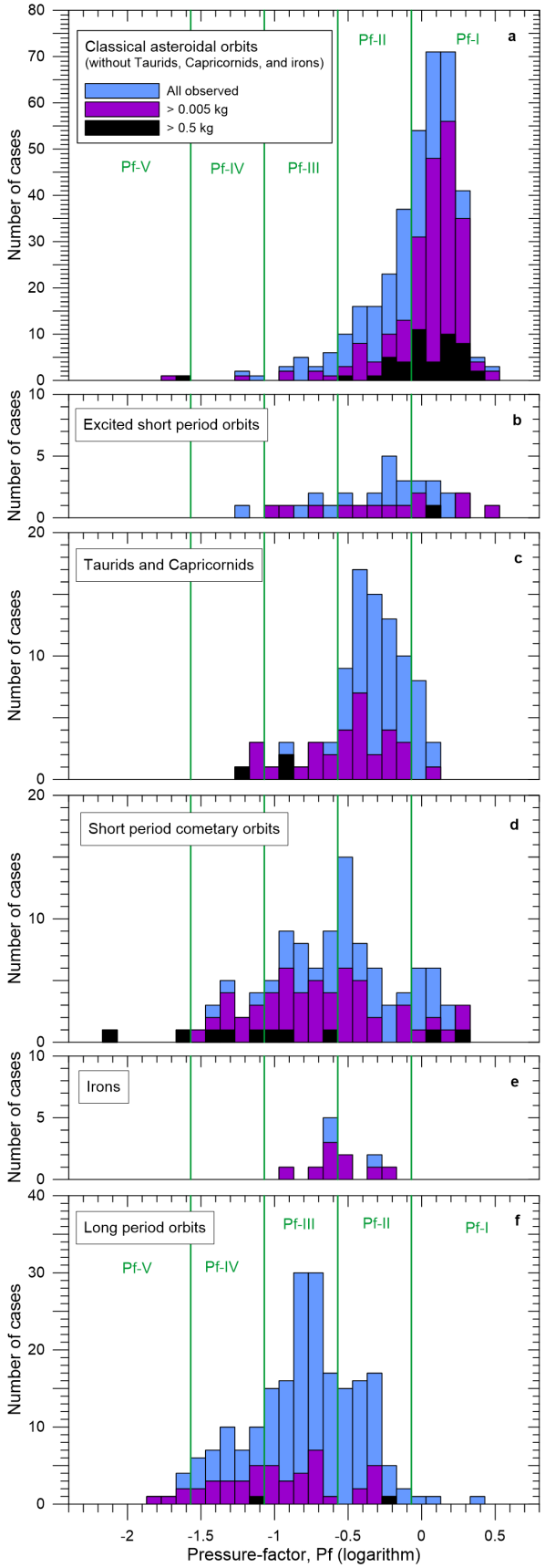

Fig. 28. Histograms of pressure factors, *Pf*, for six orbital classes. Embedded are histograms for meteoroids above a certain mass. Division into five classes of ablation ability, Pf-I to Pf-IV, is marked. See the Appendix of Paper I for the combined histogram.

7.2.2. Asteroidal material on excited orbits

One of the most surprising findings of this work is the presence or even prevalence of resistant material on orbits that can be considered cometary. These are orbits with aphelia $Q > 4.9$ AU, semimajor axes $a < 5$ AU, and either high eccentricities (and thus low perihelia) or high inclinations. We have set the boundaries at $e > 0.9$ or $i > 40°$. If both parameters are below these limits, we call the orbit a short-period cometary orbit. If at least one of the parameters is above the limit, we call the orbit an excited short-period orbit. The Tisserand parameters of the excited orbits are $T < 3$, and in many cases even $T < 2$.

In total, 31 meteoroids were observed on excited orbits. The histogram of their *Pf* values is given in Fig. 28b. The distribution is flat but most meteoroids belong to classes Pf-I and Pf-II. From seven Pf-III or Pf-IV meteoroids, three have $a > 4.5$ AU. All Pf-I meteoroids have $2.6 < a < 3.8$ AU. This is therefore the most interesting region.

It is remarkable that two of three meteoroids in the whole sample with sodium-deficient spectra fall in this region. Both EN310718_213217 and EN111118_221402 had $Q > 5$ AU, $a > 3$ AU, and $i > 70°$. The third meteoroid deficient in sodium (EN140518_005437) had a similar orbit but inclination was only 30°, so the orbit was classified as short-period cometary. Nevertheless, the meteoroid was very strong with $Pf = 2$ and can be considered as an intruder from the asteroidal population. Its spectrum was dominated by iron, while the other two sodium-deficient spectra were dominated by magnesium.

The origin of the asteroidal material on excited orbits is not clear. Despite the wide range of eccentricities and inclinations, the material may form one population. Figure 29 shows the inclinations plotted against perihelion distances. Comets and asteroids with orbits satisfying our definition of excited orbits are plotted as well. Although asteroids in these orbits are not numerous, meteoroid orbits overlap better with asteroids than comets. There are only SOHO comets with very low perihelion distances and comet 96P/Machholz 1, which has a higher inclination than meteoroids at similar perihelion distances, in this region.

The meteoroids on excited orbits also include the Southern and Northern δ Aquariids and Quadrantids (there is only one Quadrantid in our sample). With the exception of one small meteoroid, members of these showers belong to classes Pf-I and Pf-II. As shown by Sekanina & Chodas (2005), the Southern δ Aquariids, Quadrantids, SOHO comets of Marsden and Kracht groups, comet 96P, and asteroid 2003 EH1 have a common origin and form the Machholz interplanetary complex.

Our sample also contains one possible November Draconid (753 NED), a shower possibly associated with asteroid 2009 WN25 (Šegon et al. 2015). The reflectance spectrum of 2009 WN25 suggests it has cometary properties (Ieva et al. 2019) but no activity was observed. Micheli et al. (2016) associated 2009 WN25 with another shower, the November i Draconids (392 NID), but the orbital correspondence with NED is better. Interestingly, the meteoroid is one of those deficient in sodium (EN111118_221402) and with $Pf = 0.8$, it was rather strong.

Since the Machholz interplanetary complex was probably formed by cometary fragmentation (Sekanina & Chodas 2005), and asteroids such as 2003 EH1 and 2009 WN25 are supposed to be inactive cometary fragments, there is a conflict with the physical properties of meteoroids. Figure 28 shows that meteoroids in excited orbits (even with some cometary admixture) are stronger than Taurids and meteoroids in cometary orbits. One possible explanation could be that close approaches to the Sun lead to the loss of volatile sodium and to compaction of the bodies

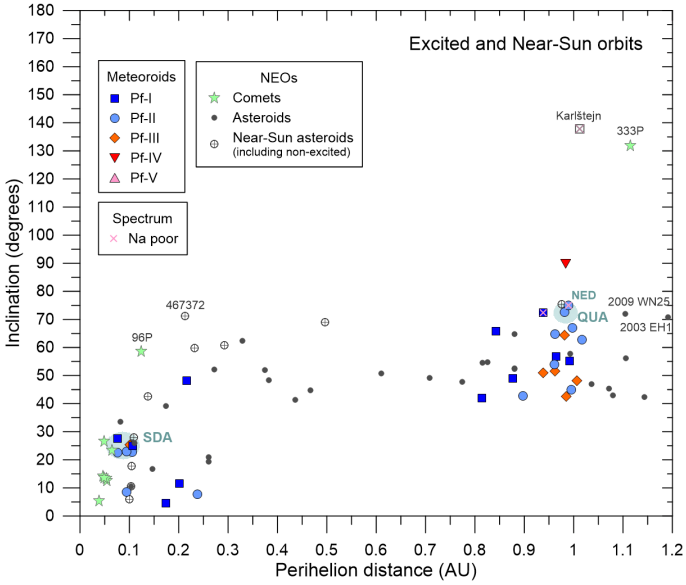

Fig. 29. Inclinations and perihelion distances of meteoroids, comets, and asteroids on excited orbits (i.e., with $Q > 4.9$ AU, $a < 5$ AU, and either $e > 0.9$ or $i > 40°$). Meteoroid Pf classes are coded by different symbols, as shown in the legend. Meteoroids with Na-poor spectra are marked. In contrast to Fig. 9, meteoroids of all masses and showers are included. The regions of Southern δ Aquariids (SDA) and Quadrantids (QUA), which overlap with November Draconids (NED), are highlighted. Near-Sun asteroids according to Emel'yanenko (2017) are included and shown by different symbols, even if they have $Q < 4.9$. The strong Karlštejn meteoroid observed in 1997 (Spurný & Borovička 1999b) is also included. For asteroid 2009 WN25, the orbit valid in 2018 was used.

(or destruction of those that are not compact). For comparison, Fig. 29 shows asteroids (including those with $Q < 4.9$ AU) that according to Emel'yanenko (2017) have recently approached the Sun within 0.1 AU. Due to the Kozai–Lidov secular perturbations, they can now have large perihelia but in that case they have high inclinations. One of them, 467372 (2004 LG), survived a perihelion distance of only 5.6 solar radii (0.026 AU), the nearest distance of any known asteroid (Vokrouhlický & Nesvorný 2012), about 3000 yr ago. 96P/Machholz was at $q \sim 0.07$ AU 4000 yr ago (Gonzi et al. 1992).

The problem with solar heating is that many meteoroids on excited orbits now have large perihelia and only those with inclination above 70° could have approached Sun within 0.1 AU in the past (using the formula for q' in Emel'yanenko 2017). Only two meteoroids with depleted sodium and one Quadrantid with an unknown spectrum have such large inclinations. Volatile sodium can be lost near the Sun due to thermal desorption (Čapek & Borovička 2009). But we also have spectra of one Southern and one Northern δ Aquariid with low perihelia, and they do contain sodium. Rudawska et al. (2016) observed one moderately bright δ Aquariid meteor with a strong sodium line and one with weak sodium. Fainter δ Aquariids were found to be completely Na-free by Borovička et al. (2005), who observed that many small meteoroids approaching the Sun within 0.2 AU have lost their sodium. The Geminids lose part of their sodium and the depletion increases with decreasing meteoroid size (Borovička et al. 2010; Abe et al. 2020). Small Quadrantids have lost sodium to lower extent than Geminids (Koten et al. 2006; Borovička et al. 2010) while the larger ones have a normal sodium content (Madiedo et al. 2016).

It is therefore common that small millimeter-sized shower meteoroids approaching the Sun are losing their sodium. In larger centimeter-sized shower meteoroids, sodium loss was not detected. Sodium loss can be expected to depend on meteoroid size, internal structure (grain size, porosity), distance to the Sun, and exposure time (Čapek & Borovička 2009). Since the atmospheric behavior of two large meteoroids depleted in sodium that we observed does not support their large porosity and the orbit does not suggest a particularly close approach to the Sun in the past (closer than for δ Aquariids), the only way to reconcile the difference seems to be a long exposure time to solar heat. The shower meteoroids are probably younger (i.e., were released from their parent bodies more recently).

Still, it is not clear whether solar heating can explain asteroidal properties of many meteoroids on excited orbits. Some of them probably never approached the Sun closer than 0.2–0.3 AU. Since the semimajor axes of most meteoroids in question are within 2.5–3.5 AU, their origin in the middle and outer asteroid belt seems possible. Their eccentricities could have been pumped up by mean motion resonances with Jupiter and some of them could have then gained high inclination due to the Kozai-Lidov perturbation.

Wiegert et al. (2020) discussed the possibility that the Marsden and Kracht groups of SOHO comets are in fact asteroidal fragments subject to the process of "supercatastrophic disruption" proposed by Granvik et al. (2016). They finally preferred cometary origin because of the cometary nature of 96P/Machholz. Nevertheless, asteroids in the outer belt also contain volatiles (Snodgrass et al. 2017) and can probably behave similar to comets when moved closer to the Sun.

In our view, the physical properties of meteoroids on excited orbits can be explained by the following hypotheses: (i) the parent bodies of a significant part or even the majority of the meteoroids on excited orbits came from the asteroid belt (middle or outer). The rest originated in Jupiter-family comets; (ii) most of the meteoroids on excited orbits either currently approach the Sun, or approached it in the past, within $\approx$ 0.3 AU. More fragile meteoroids had a higher chance of being destroyed in the vicinity of the Sun (Wiegert et al. 2020), so meteoroids representing the stronger parts of the parent bodies prevailed. The existence of this process is supported by the general lack of weak centimeter-sized meteoroids with low perihelia (see Fig. 11); and (iii) meteoroids exposed to strong solar heat for a long time can lose their sodium even if they are relatively large (centimeter-sized).

All orbits with $a < 5$ AU in our sample are prograde. However, the European Fireball Network observed a retrograde meteoroid, designated EN010697 Karlštejn, with $a = 3.49 \pm 0.09$ AU in 1997 (Spurný & Borovička 1999a,b, see also Fig. 29). That unique fireball was classified as type I, that is as a strong body, and sodium was missing in its spectrum. Its physical and chemical properties were, therefore, analogous to the extreme members of our population on excited orbits. Greenstreet et al. (2012) found that a small fraction of near-Earth asteroids can evolve into retrograde orbits and the process often involves periods of low perihelion distances and periods of high inclinations ($45° < i < 80°$). The existence of Karlštejn is therefore in accordance with the hypothesis of asteroidal origin of meteoroids on excited orbits.

The question may arise why, between 3 and 5 AU, resistant meteoroids dominate at high inclinations. One reason is that the low-inclination region contains not only asteroidal material but also young material from Jupiter-family comets. The high-inclination region contains older material that passed through the phase of low perihelion and then gained inclination through the Kozai-Lidov perturbation. Our data suggest that resistant asteroidal meteoroids have a higher chance of enduring during this process.

7.2.3. Jupiter-family orbits

The domain of Jupiter-family or, equivalently, short-period cometary orbits is in our concept at $Q > 4.9$ AU, and $a < 5$ AU, and $e < 0.9$, and $i < 40°$. The histogram of *Pf* values for meteoroids on these orbits is shown in Fig. 28d. The distribution is wide, covering all classes from Pf-I to Pf-V. For small meteoroids, the maximum of the distribution is at the boundary between Pf-II and Pf-III. For meteoroids larger than 5 g, the maximum is shifted to Pf-III. The largest bodies (>0.5 kg) are even more fragile. There are only two meteoroids in class Pf-V and both are large, but there are also meteoroids of various masses in the strongest class, Pf-I.

The *Pf* values demonstrate that most meteoroids on Jupiter-family orbits are of cometary origin. Therefore, the main meteoroid source is Jupiter-family comets. The trend of more massive meteoroids being more fragile is the same as the trend observed for the Taurids. Both small and large meteoroids are, nevertheless, shifted to lower *Pf* in comparison with Taurids. The material is therefore weaker than 2P/Encke but comparable to 169P/NEAT, the parent of α Capricornids. Some fraction of meteoroids on Jupiter-family orbits is strong and probably of mostly asteroidal origin. These orbits are intermediate between classical asteroidal and excited orbits. Asteroidal material from both of them can enter the Jupiter-family domain. We note that strong meteoroid EN140518_005437 with an unusual chemical composition, deficient in sodium and rich in iron, was on a Jupiter-family orbit but it most likely originated in the asteroid belt.

7.2.4. Long-period orbits

We call long-period orbits those with semimajor axis $a > 5$ AU. The histogram of *Pf* values in Fig. 28f shows that physical properties of meteoroids with these orbits are cometary. The maximum of the distribution is at class Pf-III and the trend of large meteoroids being weaker is present as well. The material in the strongest class, Pf-I, is rare and in this case may represent small, strong inclusions in long-period comets.

7.3. Comparison with other authors

Kresák (1969a,b) looked for differences between orbital and physical characteristics of cometary and asteroidal meteors. He considered the orbits with $i < 30°$, $q > 0.9$ AU, and $Q < 4.6$ AU to contain the highest proportion of asteroidal meteors, and those with $i < 30°$, $q > 0.9$ AU and $4.6 < Q < 10$ AU to contain exclusively cometary meteors. He found statistically significant differences in deceleration and beginning heights between these two samples. This corresponds with our finding that asteroidal material prevails on orbits with lower aphelia, although we proposed a slightly different boundary, $Q = 4.9$ AU, and there is clearly overlap between the two populations. The data used by Kresák (1969b) suggested concentrations of orbits near mean motion resonances with Jupiter, especially 3:1 and 4:1. We detected possible concentrations near 1:1 and 3:2 resonances, but the other could not be confirmed.

Ceplecha (1988) studied meteoroid populations defined, in the range of large meteoroids, by the PE criterion. Only mean

orbits were given for each population. The largest difference was in the mean eccentricity, which was found to be smallest (~ 0.6) for types I and II, intermediate (~ 0.7) for type IIIB, and largest for type IIIA. This view is obviously too simplistic. The main purpose of the Ceplecha (1988) paper was to provide absolute fluxes for each population as a function of mass. He found that cometary material prevails at masses of ~ 10 g while carbonaceous material is more abundant for both smaller (down to about 0.1 g) and larger masses. The contribution of stony material was found to be negligible below 1 g and most important between 1 and 100 kg. We did not compute absolute or even relative fluxes, but our data confirm that bodies >0.5 kg are mostly strong (see Fig. 28).

Halliday et al. (1996) presented data for 259 fireballs observed by the Canadian camera network in 1971–1985. In the data analysis, they concentrated mainly on the absolute flux estimates. Most meteoroids in the mass range 0.1–10 kg were classified as "asteroidal". In their definition, the "asteroidal group" included all fireballs with entry velocities lower than 25 km s^{-1}, with the exception of shower fireballs. For the part of the fireballs with sufficient deceleration and without obvious fragmentation, they estimated meteoroid densities. From those estimates, they concluded that as many as a quarter of the members of their "asteroidal group" are probably of cometary origin. On the other hand, their "cometary group" with velocities above 25 km s^{-1} contained some high-density objects with small perihelion distances. These observations do not contradict our results.

Matlovič et al. (2019) published an analysis of 202 bright meteors and fireballs observed by all-sky video cameras. They concentrated mostly on spectra, but orbits and physical properties of 146 meteoroids were also determined. Their plot of the Tisserand parameter, T, against the P_E parameter shows the same trends as our Fig. 4a. Namely, strong type I fireballs are encountered on orbits with $T > 2$ and only rarely on Halley-type orbits with $T < 2$. Jupiter-family orbits with $2 < T < 3$ contain both strong meteoroids, some of which are deficient in sodium, and very weak meteoroids, which are mostly large. A more detailed orbital analysis was not done. The physical properties were also evaluated using the K_B parameter, but this parameter was originally developed for smaller meteoroids (see Ceplecha 1988) and gave a more confusing picture. Matlovič et al. (2019) also noted heterogeneity in the physical properties of Perseids and other meteoroid streams. Generally, their data are in agreement with our results in the parts where both works overlap.

Wiegert et al. (2020) investigated meteoroids with low perihelia following the finding of Granvik et al. (2016) that there is a deficit of low-perihelion asteroids. Granvik et al. (2016) concluded that a super-catastrophic destruction of asteroids occurs when they reach $q = 0.076$ AU. Wiegert et al. (2020) suggested an even stricter limit for smaller bodies, since in the sample of 59 m-sized meteoroids they used, none had perihelion lower than 0.35 AU. On the contrary, an excess of low-perihelion millimeter-sized meteoroids (observed by meteor radar) was found. They proposed that asteroids and large meteoroids disintegrate into millimeter-sized particles as a result of high-speed collisions with small meteoroids near the Sun. We observe nearly the same limit, 0.07 AU, for centimeter-sized meteoroids as the one found by Granvik et al. (2016) for asteroids. Meteoroids with perihelia below 0.35 AU are relatively strong and, interestingly, the sporadic ones with $q < 0.11$ AU have perihelia concentrated in a limited range of longitudes, corresponding to the region of lowest concentration of small cometary meteoroids according to Wiegert et al. (2020). If meteoroid impacts are indeed eroding meter-sized objects below 0.35 AU, the medium-sized meteoroids we observe there may be intermediate products of this process. However, further work is needed to address this question.

Fig. 30. Comparison of the cometary fireball EN310317_023002 (*left*) and the asteroidal fireball EN181017_231532 (*right*). Both meteoroids were on cometary-type orbits with $(a, e, i) = (3.01, 0.68, 23°)$ and (3.04, 0.71, 49°), respectively. The cometary fireball appeared at heights of 98–61 km and reached a maximum absolute magnitude of −13.2. The meteoroid photometric mass was 6.7 kg. The asteroidal meteoroid was much smaller (0.04 kg) and the fireball was fainter (−7.7 mag) but longer (89–37 km). The slopes of the trajectories were almost identical (28° and 29°, respectively, to the vertical).

Shober et al. (2021) studied meteoroids on Jupiter-family orbits using data from the Desert Fireball Network. In contrast with previous works and also our results, they conclude that less than 4% of sporadic meteoroids larger than 10 g on these cometary-type orbits are of cometary origin. However, the methodology of Shober et al. (2021) contains flaws. They used the P_E criterion but substituted dynamic mass into the formula. More severely, the necessity to compute dynamic mass necessarily prevented them from including fireballs with only mild deceleration in their sample. Their approach resulted in bias since it is the cometary meteoroids that exhibit little deceleration. Figure 30 shows two fireballs with similar orbits, one classified as cometary and one as asteroidal according to the pressure factor. Despite having a larger initial mass, the cometary fireball was shorter, contained many flares, and the terminal velocity was not very different from the entry velocity (18.9 vs. 20.0 km s^{-1}). The asteroidal fireball was longer, penetrated deeper into the atmosphere, and the deceleration was significant (from 32.5 to 13.9 km s^{-1}). We conclude that the unexpected result of Shober et al. (2021) can be ascribed to the bias in their data. In fact, most orbits they included would be classified as asteroidal in our view, since despite having a Tisserand parameter < 3, they had aphelia < 4.9 AU and/or eccentricities >0.9. It is not surprising that these meteoroids had asteroidal properties. However, the authors almost completely missed the typical cometary population at $a \sim 3 - 3.5$ AU and $e \sim 0.7$, which are clearly present in our data (see Fig. 8).

In their review, Hajdukova et al. (2020) discussed the challenge of identifying interstellar meteors, that is meteors on

hyperbolic orbits. They demonstrated that although meteor databases contain a significant fraction (up to 12%) of hyperbolic orbits, and many of them with large eccentricities, none can be confirmed to be truly interstellar because of observational errors. Our sample contains 18 hyperbolic orbits (2.2%), the lowest fraction of all datasets quoted by Hajdukova et al. (2020), and their eccentricities do not exceed 1.05. It is a consequence of the better precision of our data. Only two orbits remain hyperbolic within the three sigma error. These, and perhaps some others, may be truly hyperbolic but their slight hyperbolicity was very probably acquired by processes within the Solar System. We therefore confirm the non-detection of interstellar meteoroids in the centimeter to decimeter size range. A larger sample of precise fireball orbits must be collected to set limits on their frequency.

Radiants and orbits of meteor showers have been directly compared to other sources in Sect. 4, and are not discussed here. Similarly, the frequency of meteorite falls was compared with the literature in Sect. 5.

8. Conclusions

The purpose of this extended work was the presentation and analysis of data on 824 fireballs observed by the digital cameras of the European Fireball Network in 2017–2018. Arguably, this is the most precise set of fireball orbits, atmospheric trajectories, and photometric data published so far. Despite covering only 2 yr of data, a number of new findings were obtained. The main emphasis was on the combination of orbital and physical properties, partly also supplemented with spectral data, with the aim of revealing source regions of various types of meteoroids. The most important findings are:

1. The aphelion distance, Q, is a better indicator of asteroidal origin of Earth-crossing meteoroids than the Tisserand parameter. The boundary is not strict, but sporadic meteoroids with $Q < 4.9$ AU are more likely to be asteroidal than cometary. We call such orbits classical asteroidal.
2. There are orbits containing dominantly asteroidal (i.e., physically strong) material even with $Q > 4.9$ AU. These are orbits with either high inclination ($i \gtrsim 40°$) or high eccentricity ($e \gtrsim 0.9$), and thus low perihelion distance. In both cases, the semimajor axis is $a < 5$ AU. We call these orbits excited and speculate that the material originated in the outer asteroidal belt. Part of this population is the Machholz complex containing the meteoroid streams δ Aquariids and Quadrantids.
3. All other orbits contain mostly cometary meteoroids. They can be divided into short-period or Jupiter-family orbits ($a < 5$ AU, $Q \geq 4.9$ AU, $i \leq 40°$, and $e \leq 0.9$), and long-period or Halley-type orbits ($a \geq 5$ AU, any inclination and eccentricity).
4. There are important intrusions of cometary material into classical asteroidal orbits connected with comet 2P/Encke, forming the Taurid complex, and comet 169P/NEAT, forming the Capricornid complex. Other cometary meteoroids can be encountered on asteroidal orbits as well.
5. Similarly, some meteoroids of asteroidal origin are encountered on Jupiter-family orbits.
6. On the other hand, material of high strength is rarely encountered on Halley-type orbits. If so, it probably represents strong inclusions contained in comets.
7. Parent bodies of meteoroid streams are not homogeneous and contain material with a relatively wide range of strengths. There is a trend, which is pronounced especially in Taurids but it is probably also present in other cometary streams, that large meteoroids are weaker than small ones (see also Borovička & Spurný 2020).
8. There are, nevertheless, differences among average physical properties of meteoroids from different streams. The differences are more evident when large meteoroids are compared (with masses of at least tens of grams). Capricornids and Leonids are among the weakest, and Geminids and η Virginids are among the strongest meteoroids.
9. Centimeter-sized iron meteoroids in our sample were encountered only on classical asteroidal orbits, some of them with high inclinations or low perihelia. We note that Vojáček et al. (2019) detected two small iron meteoroids on excited orbits ($a \sim 3.5$ AU, $i \sim 63°$) and Abe et al. (2020) observed three iron Geminids.
10. A couple of sodium-poor meteoroids were detected on excited orbits (with high inclination), and one sodium-poor but iron-rich meteoroid was detected on a Jupiter-family orbit. All three were physically strong.
11. No meteoroid with perihelion distance, q, lower than 0.07 AU was detected. Interestingly, all seven sporadic meteoroids with $q < 0.11$ had longitudes of perihelia, $\tilde{\omega}$, between 190° and 290°. There were also six δ Aquariids with $95° < \tilde{\omega} < 115°$. All meteoroids with low perihelia were relatively strong.
12. No clearly interstellar meteoroid was detected. A few of the observed meteoroids may have been accelerated to hyperbolic orbits within the Solar System.
13. There seems to be an excess of meteoroids in 1:1 and 3:2 mean motion resonances with Jupiter. All these resonant meteoroids have inclinations higher than 10°.
14. The orbits of Geminid meteoroids can be divided into two groups, forming a core and a wing of the stream. The core has a semimajor axis similar to Phaethon but a somewhat larger perihelion distance. The wing meteoroids have semimajor axes larger than Phaethon and perihelia similar to Phaethon. The wing meteoroids have slightly larger inclinations, on average, than those in the core.
15. The central part of the Perseid meteoroid stream is concentrated in inclination around the inclination of the parent comet 109P/Swift-Tuttle but contains some meteoroids with markedly lower perihelion distances. On the other hand, the outer part (encountered well before the shower maximum) has larger spread in inclination but a lower range of perihelion distances.
16. As already pointed out by Spurný et al. (2017) and Egal et al. (2021), the Taurid meteoroid stream contains several cataloged asteroids. We suggest that there may be a similar situation with the α Capricornid stream.
17. Meteor showers ν Draconids (220 NDR) and ξ^2 Capricornids (623 XCS), which are currently on the working list, were confirmed. Another detected shower best corresponds to the Southern October δ Arietids (28 SOA). August μ Draconids (470 AMD) were probably detected as well.
18. Fireballs with end heights below 32 km and terminal velocities below 7.5 km s^{-1} were found to be candidates for meteorite falls. Nevertheless, an analysis of the light curve and deceleration toward the end is needed in each individual case to confirm that significant mass has fallen.

Some of these findings will need confirmation or deeper elaboration using more data and more focused studies. In any case, it is encouraging that the digital cameras of the European Fireball Network are providing good data, enabling us to better understand the population of centimeter- to decimeter-sized

meteoroids in the vicinity of the Earth. As noted in Paper I, observations are continuing and more data will be published in the future.

Acknowledgements. This work was supported by grant no. 19-26232X from Czech Science Foundation and Praemium Academiae of the Czech Academy of Sciences, which provided funds for digitization of the part of the European Fireball Network. The institutional research plan is RVO:67985815.

References

Abe, S., Ogawa, T., Maeda, K., & Arai, T. 2020, Planet. Space Sci., 194, 105040
Babadzhanov, P. B. 2002, A&A, 384, 317
Bischoff, A., Barrat, J.-A., Berndt, J., et al. 2019, Geochemistry, 79, 125525
Borovička, J., & Charvát, Z. 2009, A&A, 507, 1015
Borovička, J., & Kalenda, P. 2003, Meteorit. Plan. Sci., 38, 1023
Borovička, J., & Spurný, P. 1996, Icarus, 121, 484
Borovička, J., & Spurný, P. 2008, A&A, 485, L1
Borovička, J., & Spurný, P. 2020, Planet. Space Sci., 182, 104849
Borovička, J., Popova, O. P., Nemchinov, I. V., Spurný, P., & Ceplecha, Z. 1998, A&A, 334, 713
Borovička, J., Spurný, P, Kalenda, P., & Tagliaferri, E. 2003, Meteorit. Plan. Sci., 38, 975
Borovička, J., Koten, P., Spurný, P., Boček, J., & Štork, R. 2005, Icarus, 174, 15
Borovička, J., Koten, P., Spurný, P., et al. 2010, IAU Symp., 263, 218
Borovička, J., Spurný, P., Brown, P., et al. 2013a, Nature, 503, 235
Borovička, J., Tóth, J., Igaz, A., et al. 2013b, Meteorit. Planet. Sci., 48, 1757
Borovička, J., Spurný, P., Grigore, V. I., & Svoreň, J., 2017, Planet. Space Sci., 143, 147
Borovička, J., Spurný, P., & Shrbený, L. 2019a, AJ, 160, 42
Borovička, J., Popova, O., & Spurný, P. 2019b, Meteorit. Planet. Sci., 54, 1024
Borovička, J., Bettonvil, F., Baumgarten, G. et al. 2021, Meteorit. Planet. Sci., 56, 425
Borovička, J., Spurný, P., & Shrbený, L., et al. 2022, A&A, 667, A157
Brček, A., Borovička, J., & Spurný, P. 2021, WGN, J. IMO, 49, 98
Brown, P., Weryk, R. J., Wong, D. K., & Jones, J. 2008a, Icarus, 195, 317
Brown, P., ReVelle, D. O., Silber, E. A., et al. 2008b, J. Geophys. Res., 113, E09007
Brown, P., Wong, D. K., Weryk, R. J., & Wiegert, P. 2010, Icarus, 207, 66
Brown, P., Vida, D., Moser, D. E. et al. 2019, Meteorit. Planet. Sci., 54, 2027
Čapek, D., & Borovička, J., 2009, Icarus, 202, 361
Ceplecha, Z. 1988, Bull. astr. Inst. Czechosl., 39, 221
Ceplecha, Z., & McCrosky, R. E. 1976, JGR, 81, 6257
Ceplecha, Z., Spurný, P., Borovička, J., & Keclíková, J., 1993, A&A, 279, 615
Cook, A. F. 1973, Proc. IAU Colloq. 13, eds. C. L. Hemenway, P. M. Millman, & A. F. Cook, NASA SP 319, 183
Egal, A., Wiegert, P., Brown, P. G., et al. 2021, MNRAS, 507, 2568
Emel'yanenko, V. V. 2017, Solar Syst. Res., 51, 59
Fernández, J. A., Sosa, A., Gallardo, T., & Gutiérrez, J. N. 2014, Icarus, 238, 1
Galligan, D. P., & Baggaley, W. J. 2002, Proc. IAU Colloq. 181, eds. S. F. Green et al., COSPAR Coll. Ser. 15, 48
Gonczi, R., Rickman, H., & Froeschlé, C. 1992, MNRAS, 254, 627
Granvik, M., Morbidelli, A., Jedicke, R., et al. 2016, Nature, 530, 303
Greenstreet, S., Gladman, B., Ngo, H., Granvik, M., & Larson, S. 2012, ApJ, 749, L39
Hajdukova, M., Sterken, V., Wiegert, P., & Kornoš, L. 2020, Planet. Space Sci., 192, 105060
Halliday, I., Blackwell, A. T., & Griffin, A. A. 1989a, Meteoritics, 24, 65
Halliday, I., Blackwell, A. T., & Griffin, A. A. 1989b, Meteoritics, 24, 173
Halliday, I., Griffin, A. A., & Blackwell, A. T. 1996, Meteorit. Planet. Sci., 31, 185
Hasegawa, I. 2001, in Proc. Meteoroids 2001 Conf., ed. B. Warmbein, ESA-SP 495, 55
Hildebrand, A. R., McCausland, P. J. A., Brown, P. G., et al. 2006, Meteorit. Planet. Sci., 41, 407
Holman, D., & Jenniskens, P. 2012, WGN, J. IMO, 40, 36
Ieva, S., Micheli, M., Perna. D., et al. 2019, MNRAS, 487, 2335
Jenniskens, P. 2006, Meteor Showers and their Parent Comets (Cambridge: Cambridge University Press)
Jenniskens, P., & Vaubaillon, J. 2010, AJ, 139, 1822
Jenniskens, P., Nénon, Q., Albers, J., et al. 2016a, Icarus, 266, 331
Jenniskens, P., Nénon, Q., Gural, P. S., et al. 2016b, Icarus, 266, 355
Jopek, T. J., & Kaňuchová, Z. 2017, Planet. Space Sci., 143, 3
Jopek, T. J., Valsecchi, G. B., & Froeschlé, Cl. 2003, MNRAS, 344, 665
Kokhirova, G. I., & Borovička, J. 2011, A&A, 533, A115
Kornoš, L., Matlovič, P., Rudawska, R., et al. 2014, in Proc. Meteoroids 2013 Conf., eds. T. J. Jopek, et al., A. Mickiewicz Univ. Press., Poznań, 225
Koten, P., Borovička, J., Spurný, P., et al. 2006 MNRAS, 366, 1367
Kresák, Ľ. 1969a, Bull. astr. Inst. Czechosl., 20, 177
Kresák, Ľ. 1969b, Bull. astr. Inst. Czechosl., 20, 231
Kresák, Ľ., & Porubčan, V. 1970, Bull. astr. Inst. Czechosl., 21, 153
Madiedo, J. M., Espartero, F., Trigo-Rodríguez, J. M., et al. 2016, Icarus, 275, 193
Matlovič, P., Tóth, J., Rudawska, R., Kornoš, L., & Pisarčíková, A. 2019, A&A, 629, A71
Meech, K. J., Kleyna, J., Hainaut,O. R., et al. 2013, Icarus, 222, 662
Micheli, M., Tholen, D. J., & Jenniskens, P. 2016, Icarus, 267, 64
Mills, T., Brown, P. G., Mazur, M. J. et al. 2021, MNRAS, 508, 3684
Molau, S., & Rendtel, J. 2009, WGN, J. IMO, 37, 98
Moorhead, A. V., Clements, T., & Vida, D. 2021, MNRAS, 508, 326
Popova, O., Borovička, J., Hartmann, W. K., et al. 2011, Meteorit. Planet. Sci., 46, 1525
Rudawska, R., & Jenniskens, P. 2014, in Proc. Meteoroids 2013 Conf., eds. T. J. Jopek et al. (Poznań: A. Mickiewicz Univ. Press), 217
Rudawska, R., Tóth, J., Kalmančok, D., Zigo, P., & Matlovič, P. 2016, Planet. Space Sci., 123, 25
Ryabova, G. O. 2021, MNRAS, 507, 4481
Ryabova, G. O. 2022, Planet. Space Sci., 210, 105378
Šegon, D. Gural, P., Andreić, Ž, et al. 2015, WGN, J. IMO, 43, 147
Sekanina, Z., & Chodas, P. W. 2005, ApJS, 161, 551
Shaddad, M. H., Jenniskens, P., Numan, D., et al. 2010, Meteorit. Planet. Sci., 45, 1557
Shiba, Y. 2017, WGN, J. IMO, 45, 127
Shober, P. M., Sansom, E. K., Bland, P. A., et al. 2021, Planet. Sci. J., 2, 98
Snodgrass, C., Agarwal, J., Combi, M. et al. 2017, A&AR, 25, 5
SonotaCo 2009, WGN, J. IMO, 37, 55
Southworth, R. B., & Hawkins, G. S., 1963, Smithson. Contrib. Astrophys., 7, 261
Spurný, P., & Borovička, J. 1999a, in: Meteoroids 1998, eds. W. J. Baggaley, & V. Porubčan (Bratislava, Slovakia: Astron. inst. Slovak Acad. Sci.), 143
Spurný, P., & Borovička, J. 1999b, in: Evolution and Source Regions of Asteroids and Comets, eds. J. Svoreň et al., IAU Colloq. 173, 163
Spurný, P., & Borovička, J., 2019, Meteoroids 2019 Conf., Bratislava, Slovakia, June 17–21, 2019, 8
Spurný, P., Oberst, J., & Heinlein, D. 2003, Nature, 423, 151
Spurný, P., Haloda, J., Borovička, J., et al. 2014, A&A, 570, A39
Spurný, P., Borovička, J., Mucke, H., & Svoreň, J. 2017, A&A, 605, A68
Spurný, P., Borovička, J., & Heinlein, D., 2019, Meteoroids 2019 conf., Bratislava, Slovakia, June 17–21, 2019
Spurný, P., Borovička, J., Shrbený, L., et al. 2020, Meteorit. Planet. Sci., 55, 376
Tancredi, G. 2014, Icarus, 233, 66
Trigo-Rodríguez, J. M., & Llorca, J. 2006, MNRAS, 372, 655
Trilling, D. E., Hora, J. L., Mommert, M., et al. 2017, AAS DPS meeting, 49, 110.06
Vida, D., Šegon, D., Gural, P. S., et al. 2021, MNRAS, 506, 5046
Vojáček, V., Borovička, J., Koten, P., Spurný, P., & Štork, R. 2019, A&A, 621, A68
Vojáček, V., Borovička, J., Spurný, P., & Čapek, D. 2020, Planet. Space Sci., 184, 104882
Vokrouhlický, D., & Nesvorný, D. 2012, A&A, 541, A109
Wiegert, P., Clark, D., Campbell-Brown, M., & Brown, P. 2017, Central Bureau Electronic Telegrams, 4415
Wiegert, P., Brown, P., Pokorný, P., et al. 2020, AJ, 159, 143
Ye, Q.-Z., 2018, Planet. Space Sci., 164, 7

Appendix A: Additional tables

Table A.1. Fireballs possibly associated with the Northern or Southern δ Cancrids (96 NCC and 97 SCC). Selected orbital elements and the pressure factor are given. Orbital elements from the literature are given at the bottom.

Code	q	e	i	Ω	Pf
EN070117_235400	0.365	0.774	0.57	287.45	1.0
EN200117_181106	0.546	0.753	2.77	120.69	1.3
EN200117_192130	0.520	0.768	2.03	120.75	1.6
EN200117_234318	0.528	0.775	0.09	299.71	2.0
EN290117_033628	0.521	0.806	1.44	129.25	0.22
δ Cancrids [1]	0.45	0.80	0	296	
NCC [2]	0.410	0.814	2.7	290.0	
SCC [2]	0.430	0.811	4.7	109.3	

Notes. [1] Cook (1973), [2] Jenniskens et al. (2016a)

Table A.2. Fireballs associated with the σ Hydrids (16 HYD), July γ Draconids (184 GDR), and κ Ursae Majorids (445 KUM).

Code	q	e	i	Ω	Pf
EN071217_025105	0.234	0.973	126.92	74.94	0.40
EN071217_230112	0.236	0.999	127.89	75.79	0.40
HYD [1]	0.237	0.978	126.5	79.1	
HYD [3]	0.257	0.985	128.7	76.5	
HYD [4]	0.249	0.970	128.3	78.47	
EN280717_235801	0.980	0.999	41.72	125.85	0.42
EN290717_212641	0.980	0.993	40.19	126.70	0.39
GDR [2]	0.978	0.972	40.24	124.66	
GDR [3]	0.977	0.967	40.3	124.7	
GDR [4]	0.978	0.966	40.28	125.62	
EN051118_215131	0.987	0.981	129.98	223.17	0.032
EN061118_190859	0.988	0.986	129.38	224.06	0.038
KUM [3]	0.988	1.000	129.6	224.0	
KUM [4]	0.983	0.890	129.0	224.49	

Notes. [1] Jopek et al. (2003), [2] Holman & Jenniskens (2012), [3] Jenniskens et al. (2016a), [4] Vida et al. (2021).

Table A.3. Fireballs possibly associated with the ν Draconids (220 NDR).

Code	q	e	i	Ω	Pf
EN100917_225415	1.006	0.665	33.35	168.17	0.30
EN090918_000545	1.007	0.675	35.00	166.03	0.41
EN110918_231100	1.005	0.700	27.53	168.91	0.099
EN170918_010734	0.998	0.665	24.92	173.86	0.30
EN180918_030212	1.002	0.606	30.17	174.91	1.4
NDR [1]	1.004	0.654	28.8	171.7	

Notes. [1] Jenniskens et al. (2016b).

Table A.4. Fireballs possibly associated with the Southern δ Piscids (216 SPI), Southern October δ Arietids (28 SOA), or ξ Arietids (624 XAR).

Code	q	a	i	Ω	Pf
EN150918_231506	0.234	2.31	8.36	352.80	1.8
EN290917_030848	0.243	1.85	7.61	5.94	0.83
EN081018_224959	0.234	1.75	7.17	15.35	0.51
EN101018_023945	0.256	1.93	6.34	16.50	0.79
EN131018_020534	0.282	1.44	4.97	19.45	0.67
EN151017_012737	0.262	1.71	6.14	21.66	0.57
SPI [1]	0.251	1.45	5.6	353.9	
SOA [1]	0.286	1.75	5.7	15.4	
XAR [1]	0.312	1.86	5.7	24.4	

Notes. [1] Jenniskens et al. (2016a).

Table A.5. Fireballs possibly associated with the August μ Draconids (470 AMD) and ξ^2 Capricornids (623 XCS).

Code	q	e	i	Ω	Pf
EN140817_193344	1.013	0.658	35.79	141.95	0.29
EN240817_235428	1.010	0.657	34.78	151.75	0.19
EN260817_185317	1.006	0.677	31.97	153.48	1.1
AMD [1]	1.011	0.654	30.3	145.4	
AMD [2]	1.012	0.631	29.5	144.4	
AMD [3]	1.009	0.648	33.8	149.5	
EN190717_002210	0.463	0.796	7.47	116.32	0.069
EN190717_011014	0.471	0.805	8.02	116.35	0.18
EN190718_223059	0.476	0.805	7.94	116.96	0.058
XCS [3]	0.509	0.786	7.6	119.7	

Notes. [1] Rudawska & Jenniskens (2014), [2] Kornoš et al. (2014), [3] Jenniskens et al. (2016a).

Table A.6. Orbit of asteroid 2019 DN and three fireballs with similar orbits.

Code	a	q	i	ω	Ω	D_{SH}
2019 DN	2.43	1.01	2.9	162.2	357.0	
EN240317_212628	2.41	0.99	1.0	167.6	4.2	0.045
EN310317_015155	2.20	1.00	1.3	175.9	10.3	0.050
EN040318_224701	2.34	0.99	1.9	177.0	344.0	0.035